

C^1 -continuous space-time discretization based on Hamilton's law of varying action

Janine C. Mergel^a, Roger A. Sauer^{a,*}, Sina Ober-Blöbaum^b

^a*AICES Graduate School, RWTH Aachen University, Templergraben 55, 52056 Aachen, Germany*

^b*Department of Engineering Science, University of Oxford, Parks Road, Oxford, OX1 3PJ, UK*

Abstract

We develop a class of C^1 -continuous time integration methods that are applicable to conservative problems in elastodynamics. These formulations are based on Hamilton's law of varying action. From the action integral of the continuous system we derive a spatially and temporally weak form of the governing equilibrium equations. This expression is first discretized in space, considering standard finite elements. The resulting system is then discretized in time, approximating the displacement by piecewise cubic Hermite shape functions. Within the time domain we thus achieve C^1 -continuity for the displacement field and C^0 -continuity for the velocity field. From the discrete virtual action we finally construct a class of different one-step schemes. These methods are examined both analytically and numerically. Here, we study both linear and nonlinear systems, considering either inherently continuous or discrete structures. In the numerical examples we focus on one-dimensional applications. The provided theory, however, is general and valid also for problems in 2D or 3D. We show that the most favorable candidate — denoted as pp-scheme — converges with order four. Thus, especially if high accuracy of the numerical solution is required, this scheme can be more efficient than existing methods. It further exhibits similar properties as variational integrators: Conservation of linear momentum and, for simple linear systems, symplecticity. While it remains to be investigated whether our method is symplectic for arbitrary systems, all our numerical results show an excellent long-term energy behavior.

Keywords: Hamilton's law of varying action, Hamilton's principle, Hermite interpolation, nonlinear elastodynamics, symplectic integration, variational integrators

1. Introduction

In this work we derive a class of time integration methods for the computational analysis of deformable solids. We consider a discrete version of Hamilton's law of varying action to obtain space-time discretization schemes based on cubic Hermite functions in time.

*Corresponding author

Email addresses: mergel@aices.rwth-aachen.de (Janine C. Mergel), sauer@aices.rwth-aachen.de (Roger A. Sauer), sina.ober-blobaum@eng.ox.ac.uk (Sina Ober-Blöbaum)

1.1. Overview of existing methods

One very common approach for the numerical analysis of elastodynamic problems is the application of so-called semi-discrete procedures: Here, the (spatially and temporally) continuous system is discretized in space and time separately. First, the mechanical equilibrium equations — describing the deformation of the body — are discretized in space by means of the finite element method (FEM). At this point we refer to any standard literature on nonlinear finite elements for solids; see e.g. Ref. [8, 71, 73]. The spatially discrete system is then discretized in time, using for instance a finite difference scheme or collocation based on Taylor series expansion. Discretization schemes of this type include many well-known methods, such as the Newmark algorithm [55], the HHT- α method [30], the WBZ- α method [70], or the generalized- α method [13]. Besides methods fulfilling the equilibrium equations at single time steps, there exist various approaches based on weighted residuals; these consider equilibrium in an weighted-average sense and go back to the publication by Zienkiewicz [72]. A weighted residual approach based on cubic Hermite interpolation in time, for instance, is discussed by Fung [20]. See also the generalized method proposed by Modak and Sotelino [54]. In addition, there exists a broad literature on methods combining finite elements (FE) in both space and time. In general, these solution schemes can be constructed by forming a (spatially and temporally) weak form of the equations of motion, and discretizing the resulting statement by means of finite elements. The first approaches accounting for finite elements in time go back to Argyris and Scharpf [1], Oden [59], and Fried [19]. Early publications on space-time FE methods include Ref. [34, 36, 37]. A broader literature review on time integration methods in general can be found e.g. in Ref. [7, 9, 24].

A special class of time integration schemes applied to mechanical systems is formed by geometrical integrators. Geometric integration enables the design of robust methods that provide both quantitatively and qualitatively accurate results. Since these methods preserve the geometric properties of the flow of a differential equation, they are able to exactly represent the main characteristic properties of the physical process; see e.g. Marsden and West [53], Hairer et al. [25], and Reich [60]. Geometric integration methods can be mainly divided into two classes: 1) Energy-momentum integrators (see Simo and Tarnow [65], Simo et al. [66], Gonzalez [23], Besch and Steinmann [9], Groß et al. [24], Hesch and Betsch [28, 29], Gautam and Sauer [21] and Krenk [42]), and 2) symplectic momentum-conserving integrators. The first class of methods fulfills the conservation laws of energy and momentum automatically. The second class preserves both the symplectic form and — in the presence of symmetries — momentum maps; it additionally shows excellent long-term energy behavior. Symplectic-momentum integrators can be represented by the class of variational integrators [53, 67]. For conservative systems, these methods are constructed by forming a discrete version of Hamilton's principle, choosing both a finite-dimensional function space and a suitable numerical quadrature. See Ref. [47, 48] for an overview. For dissipative or controlled mechanical systems, they can be derived from a discrete version of the Lagrange-d'Alembert principle [39, 56]. Within the last years variational integrators have been extended towards constrained [14, 40, 49, 51], non-smooth [18, 38], stochastic [11], multirate and

multiscale [50, 68] systems as well as to electric circuits [58]. For variational integrators in combination with spatial discretization we refer to Lew et al. [46], Demoures et al. [17], Wolff and Buchner [69], and the references therein. Besides these semi-discrete approaches, there exists a covariant space-time discretization method by Marsden et al. [52]. This multi-symplectic scheme allows for symplecticity in both space and time.

In most of the previously mentioned work the solution is approximated by using piecewise Lagrange interpolation. For a mechanical system, this leads to a smooth approximation of the position, but to discontinuities in the velocity at the discrete time steps. Besides this approach, Leok and Shingel [45] have developed a variational integrator based on piecewise Hermite interpolation. In their prolongation-collocation approach, not only the solution of the discrete Euler-Lagrange equations, but also its time derivatives are approximated with sufficient accuracy. This leads to a globally smooth approximation of the solution. Note that Ref. [45] does not include the combined discretization in both space and time.

To incorporate any initial conditions of the mechanical system explicitly, early publications on structural dynamics have considered the so-called Hamilton’s law of varying action; see e.g. Argyris and Scharpf [1], Fried [19], Bailey [2–5], Simkins [63, 64], and Borri et al. [10]. This law can be regarded as a generalization of Hamilton’s principle; it accounts for any initial and final velocities by considering non-zero variations in the displacement at the boundaries of the time domain. Some of the studies mentioned above also include cubic Hermite interpolation in time for the displacement. Based on this law, a family of methods has been proposed [6, 62] that combines different zero-variations of the displacement or velocity at initial and final time. In addition, G eradin [22] has constructed from a subsequent application of Hamilton’s law a time integration method based on Hermite interpolation. While variational integrators are automatically symplectic (due to the discretized action integral serving as generating function [25]), it is not clear if the same properties hold for integration schemes constructed from Hamilton’s law.

1.2. Objectives

In this paper we derive a class of space-time integration methods that are based on piecewise cubic Hermite interpolation in time. We therefore consider Hamilton’s law of varying action: Thus, any initial velocities can be accounted for in the formulation explicitly. Using a semi-discrete approach, we first discretize our resulting equilibrium equation in space and then in time. Instead of deriving additional conditions on the time derivatives of the approximated solution — as it is done in the approach of Leok and Shingel [45] — we consider independent variations of the position and velocities.

In general, one could then construct a variational integrator by 1) varying the action of the entire temporal domain, and 2) deriving from the variation a set of discrete Euler-Lagrange equations. Since for a cubic Hermite approximation, however, this would lead to an (unconditionally) unstable numerical method, we pursue a different approach: We vary the action for each discrete time interval individually, which leads

to an overdetermined system of four equations. By choosing different combinations of equations, we derive a family of six different one-step methods. One of these schemes coincides with the method proposed by G eradin [22].

In fact, our time integration methods are not variational in the sense that they are not derived from the virtual action of the total time domain. We will demonstrate, however, that the most favorable of our schemes — denoted in the following as pp-scheme — shows similar properties like true variational integrators: Conservation of linear momentum and, for a simple harmonic oscillator, symplecticity. Interestingly, this is not the case for the variant discussed in Ref. [22].

Note that like other methods based on C^1 -continuous approximations in time, our integration schemes are not favorable for the simulation of discontinuous changes (such as shock waves) in mechanical systems. Instead, we apply the pp-scheme to numerically investigate temporally smooth examples; these include both linear and nonlinear as well as intrinsically discrete and spatially continuous problems. Here, we focus on one-dimensional applications; the theory, however, is also valid for conservative systems in 2D and 3D. Compared to both the formulation of G eradin and the method of Leok and Shingel based on cubic Hermite interpolation, our pp-scheme exhibits a higher order of convergence. In addition, based on the desired accuracy, it may be more efficient than collocation methods like the Newmark algorithm.

1.3. Outline

The remainder of this paper is structured as follows. Section 2 introduces the action integral of a continuous body deforming over time. From Hamilton’s law of varying action a (spatially and temporally) weak form of the mechanical equilibrium equation is derived. Section 3 briefly outlines its spatial discretization by means of standard finite elements. The temporal discretization is discussed in Section 4, providing a solution strategy that leads to a class of different integration methods. These methods are then related to other approaches from the literature. In Section 5, we study the main characteristic properties of our integration schemes, such as symplecticity and the long-term and convergence behavior. The most favorable scheme is then applied to investigate several numerical examples (Section 6). Section 7 finally concludes this paper.

2. Hamilton’s law of varying action

In this section we summarize the continuum mechanical equations describing a body undergoing finite motion and deformation. For the general theory of continuum mechanics, the reader is referred to text books [12, 31]. Consider a body deforming within the time domain $[0, T]$. In the initial configuration, at $t = 0$, the body is denoted by \mathcal{B}_0 ; its boundary is denoted by $\partial\mathcal{B}_0$. The body can be subjected to volumetric loads, $\bar{\mathbf{B}}$ (applied in \mathcal{B}_0), deformations, $\bar{\varphi}$ (prescribed on $\partial_\varphi\mathcal{B}_0 \subseteq \partial\mathcal{B}_0$), and surface loads, $\bar{\mathbf{T}}$

(applied on $\partial_t \mathcal{B}_0 \subseteq \mathcal{B}_0$).¹ At any time $t \in (0, T]$, the deformation of the body is characterized by a unique mapping of a material point, $\mathbf{X} \in \mathcal{B}_0$, to its current position, $\mathbf{x} = \boldsymbol{\varphi}(\mathbf{X}, t) \in \mathcal{B}$. The material time derivative $\mathbf{v} := \partial \mathbf{x} / \partial t$ corresponds to the velocity of a material particle located at \mathbf{x} ; in short we will also write $\mathbf{v} = \dot{\mathbf{x}}$.

2.1. Action of the continuous system

In the following we assume 1) conservation of mass, 2) hyperelastic material behavior, and 3) that the external forces are independent of the deformation. We derive our time integration schemes from the action integral of the continuous system, defined as

$$\mathcal{S} = \int_0^T L(\mathbf{x}, \mathbf{v}) dt. \quad (1)$$

The integrand corresponds to the Lagrangian of our system, given by

$$L(\mathbf{x}, \mathbf{v}) = K(\mathbf{v}) - \Pi(\mathbf{x}), \quad \Pi(\mathbf{x}) = \Pi_{\text{int}}(\mathbf{x}) - \Pi_{\text{ext}}(\mathbf{x}). \quad (2)$$

Here, K is the kinetic energy and Π is the potential energy due to both internal strains and external forces; these terms are given by

$$K(\mathbf{v}) = \frac{1}{2} \int_{\mathcal{B}_0} \rho_0 \mathbf{v} \cdot \mathbf{v} dV, \quad (3)$$

$$\Pi_{\text{int}}(\mathbf{x}) = \int_{\mathcal{B}_0} W(\mathbf{x}) dV, \quad (4)$$

$$\Pi_{\text{ext}}(\mathbf{x}) = \int_{\mathcal{B}_0} \mathbf{x} \cdot \rho_0 \bar{\mathbf{B}} dV + \int_{\partial_t \mathcal{B}_0} \mathbf{x} \cdot \bar{\mathbf{T}} dA. \quad (5)$$

The terms ρ_0 and $W(\mathbf{x})$ respectively denote the material density (in the initial configuration) and an energy density function characterizing the material behavior; a detailed description of $W(\mathbf{x})$ for different material models can be found e.g. in Ref. [8, 71, 73].

2.2. Variation of the action

We now consider an admissible variation of the deformation, $\delta \mathbf{x} \in \mathcal{V}$,

$$\mathcal{V} = \left\{ \delta \mathbf{x} : \mathcal{B}_0 \times [0, T] \rightarrow \mathbb{R}^d \mid \delta \mathbf{x}(\mathbf{X}, t) |_{\partial_\varphi \mathcal{B}} = \mathbf{0} \right\}. \quad (6)$$

Here, d is the dimension of Euclidean space. Varying the action integral (1) yields

$$\delta \mathcal{S} = \int_0^T \delta L(\mathbf{x}, \mathbf{v}) dt, \quad \delta L(\mathbf{x}, \mathbf{v}) = \delta K(\mathbf{v}) - [\delta \Pi_{\text{int}}(\mathbf{x}) - \delta \Pi_{\text{ext}}(\mathbf{x})], \quad (7)$$

¹We assume that $\partial_\varphi \mathcal{B}_0 \cup \partial_t \mathcal{B}_0 = \partial \mathcal{B}_0$ and $\partial_\varphi \mathcal{B}_0 \cap \partial_t \mathcal{B}_0 = \emptyset$.

where the variations of the energy terms are given by

$$\delta K(\mathbf{v}) = \int_{\mathcal{B}_0} \delta \mathbf{v} \cdot \rho_0 \mathbf{v} \, dV, \quad (8)$$

$$\delta \Pi_{\text{int}}(\mathbf{x}) = \int_{\mathcal{B}} \text{grad } \delta \mathbf{x} : \boldsymbol{\sigma} \, dv, \quad (9)$$

$$\delta \Pi_{\text{ext}}(\mathbf{x}) = \int_{\mathcal{B}_0} \delta \mathbf{x} \cdot \rho_0 \bar{\mathbf{B}} \, dV + \int_{\partial_t \mathcal{B}_0} \delta \mathbf{x} \cdot \bar{\mathbf{T}} \, dA. \quad (10)$$

The tensor $\boldsymbol{\sigma}$ denotes the Cauchy stress, which is derived from the strain energy density function, W , appearing in Eq. (4).

If we enforce the deformation at $t = 0$ and $t = T$ to be fixed (s.t. the variations $\delta \mathbf{x}(0)$ and $\delta \mathbf{x}(T)$ become zero), we arrive at the classical Hamilton's principle,

$$\delta \mathcal{S} = 0 \quad \forall \delta \mathbf{x} \in \left\{ \delta \mathbf{x} \in \mathcal{V} \mid \delta \mathbf{x}(\mathbf{X}, 0) = \mathbf{0}, \delta \mathbf{x}(\mathbf{X}, T) = \mathbf{0} \right\}, \quad (11)$$

see e.g. the book by Lanczos [43]. Instead, however, we leave the variations $\delta \mathbf{x}(0)$ and $\delta \mathbf{x}(T)$ arbitrary for now. In this case, $\delta \mathcal{S}$ is equal to the following boundary term evaluated at $t = 0$ and $t = T$:

$$\delta \mathcal{S} = \left\langle \delta \mathbf{x}, \frac{\partial L(\mathbf{x}, \mathbf{v})}{\partial \mathbf{v}} \right\rangle \Big|_0^T \quad \forall \delta \mathbf{x} \in \mathcal{V}. \quad (12)$$

The term in angle brackets corresponds to the scalar product of the variation, $\delta \mathbf{x}$, and the linear momentum of the body, i.e.

$$\left\langle \delta \mathbf{x}, \frac{\partial L(\mathbf{x}, \mathbf{v})}{\partial \mathbf{v}} \right\rangle = \int_{\mathcal{B}_0} \delta \mathbf{x} \cdot \rho_0 \mathbf{v} \, dV. \quad (13)$$

A more detailed discussion of arbitrary variations at the boundaries can be found in Ref. [43] (see Chapter V.3 there). Due to the scalar product, Eq. (12) depends on the system's initial momentum (and thus on its initial velocity) explicitly. This is the reason why expression (12) has been discussed in several early publications studying initial value problems in structural dynamics, such as Ref. [1–3, 6, 63, 64]. Following the terminology used in several of these papers, we refer to Eq. (12) as ‘Hamilton's law of varying action’. A very interesting comment on its origin can be found in a paper by Bailey (Ref. [3], p. 434): ‘When copies of Hamilton's original papers [26, 27] were obtained, it was found that Hamilton had furnished what he called the ‘law of varying action’. He did not furnish what is now known as ‘Hamilton's principle’. Evidently, in the latter part of the 19th century, application of the concepts of the variational calculus of Euler and Lagrange reduced Hamilton's law to Hamilton's principle.’

Equation (12) represents the (spatially and temporally) weak form of the governing equilibrium equations. Note that this expression is general and valid for elastodynamic problems in \mathbb{R}^d , $d = \{1, 2, 3\}$. Nevertheless, since we focus on the development and analysis of a new time integration method, we numerically investigate only one-dimensional problems with $\delta \Pi_{\text{ext}} = 0$ in this paper. A detailed study of time-dependent problems in both 2D or 3D may be the subject of future work.

3. Spatial discretization

We now briefly outline the spatial discretization of the governing equations by means of the finite element method. Regarding nonlinear finite elements for solids we refer to text books such as Ref. [8, 71, 73]. We spatially discretize Eq. (12) by using n_{el} finite elements; for each element, Ω^e , both the initial position, \mathbf{X} , and the deformation, $\mathbf{x}(\mathbf{X}, t)$, are approximated by means of

$$\mathbf{X}^h(\mathbf{X}) = \mathbf{N}_e(\mathbf{X}) \mathbf{X}_e, \quad \mathbf{x}^h(\mathbf{X}, t) = \mathbf{N}_e(\mathbf{X}) \mathbf{x}_e(t). \quad (14)$$

The vectors

$$\mathbf{X}_e = \begin{bmatrix} \mathbf{X}_1 \\ \vdots \\ \mathbf{X}_{n_{ne}} \end{bmatrix} \quad \text{and} \quad \mathbf{x}_e(t) = \begin{bmatrix} \mathbf{x}_1(t) \\ \vdots \\ \mathbf{x}_{n_{ne}}(t) \end{bmatrix} \quad (15)$$

contain the initial and current positions of those n_{ne} nodes belonging to element Ω^e . Note that these quantities are still continuous with respect to time. The array $\mathbf{N}_e = [N_1 \mathbf{I}_d, \dots, N_{n_{ne}} \mathbf{I}_d]$ contains the nodal shape functions associated with Ω^e . Consequently, we obtain for the discrete velocity

$$\mathbf{v}^h(\mathbf{X}, t) = \mathbf{N}_e(\mathbf{X}) \dot{\mathbf{x}}_e(t), \quad (16)$$

where the dot indicates the derivative with respect to time. Using an isoparametric concept, we discretize the variations by means of the same shape functions,

$$\delta \mathbf{x}^h(\mathbf{X}, t) = \mathbf{N}_e(\mathbf{X}) \delta \mathbf{x}_e(t), \quad \delta \mathbf{v}^h(\mathbf{X}, t) = \mathbf{N}_e(\mathbf{X}) \delta \dot{\mathbf{x}}_e(t). \quad (17)$$

We can further write

$$\text{grad } \delta \mathbf{x}^h = \mathbf{B}_e(\mathbf{X}) \delta \mathbf{x}_e(t) \quad (18)$$

for a suitable definition of the strain operator \mathbf{B}_e . By inserting these relations into Eq. (12) and (13), we obtain

$$\delta \mathcal{S}^h = \sum_{e=1}^{n_{el}} \left[\delta \mathbf{x}_e^T \mathbf{m}_e \dot{\mathbf{x}}_e \right] \Big|_0^T, \quad (19)$$

where $\delta \mathcal{S}^h$ can be computed from

$$\delta \mathcal{S}^h = \int_0^T \delta L^h(\mathbf{x}, \dot{\mathbf{x}}) dt, \quad \delta L^h(\mathbf{x}, \dot{\mathbf{x}}) = \sum_{e=1}^{n_{el}} [\delta \dot{\mathbf{x}}_e^T \mathbf{m}_e \dot{\mathbf{x}}_e - \delta \mathbf{x}_e^T \mathbf{f}^e]; \quad (20)$$

cf. Eq. (7) – (10). Here, the vectors $\mathbf{x}(t)$ and $\dot{\mathbf{x}}(t)$ denote the deformation and velocity at all spatial FE nodes. The elemental mass matrices, \mathbf{m}_e , and the force vectors, $\mathbf{f}^e := \mathbf{f}_{\text{int}}^e - \mathbf{f}_{\text{ext}}^e$, are computed through

$$\mathbf{m}_e := \int_{\Omega_0^e} \rho_0 \mathbf{N}_e^T \mathbf{N}_e dV, \quad (21)$$

$$\mathbf{f}_{\text{int}}^e := \int_{\Omega^e} \mathbf{B}_e^T \boldsymbol{\sigma} dv, \quad (22)$$

$$\mathbf{f}_{\text{ext}}^e := \int_{\Omega_0^e} \rho_0 \mathbf{N}_e^T \bar{\mathbf{B}} dV + \int_{\Gamma_{0t}^e} \mathbf{N}_e^T \bar{\mathbf{T}} dA, \quad (23)$$

introducing $\Gamma_{\partial t}^e = \Omega_0^e \cap \partial_t \mathcal{B}_0^h$. To obtain a shorter notation we will later refer to the global mass matrix, \mathbf{m} , and the global force vectors, $\mathbf{f} := \mathbf{f}_{\text{int}} - \mathbf{f}_{\text{ext}}$, assembled from the elemental contributions.

Equation (19) finally corresponds to the spatially discrete version of Hamilton's law of varying action.

4. Temporal discretization

We now discretize the (spatially discrete) virtual action, $\delta \mathcal{S}^h$, in time. To achieve temporal C^1 -continuity, we approximate the nodal deformation of element Ω^e by cubic Hermite shape functions; $\mathbf{x}_e(t) \approx \mathbf{x}_e^t(t)$ with

$$\mathbf{x}_e^t(t) = R_1(t) \hat{\mathbf{x}}_n^e + R_2(t) \hat{\mathbf{x}}_{n+1}^e + H_1(t) \hat{\mathbf{v}}_n^e + H_2(t) \hat{\mathbf{v}}_{n+1}^e, \quad t \in [t_n, t_{n+1}], \quad (24)$$

where $n = 0, \dots, N-1$, $t_0 = 0$, and $t_N = T$. The vectors $\hat{\mathbf{x}}_n^e$ and $\hat{\mathbf{x}}_{n+1}^e$ contain the nodal deformations at t_n and t_{n+1} ; the vectors $\hat{\mathbf{v}}_n^e$ and $\hat{\mathbf{v}}_{n+1}^e$ are the corresponding nodal velocities. See [Appendix A.1](#) for the definition of the shape functions R_1 , R_2 , H_1 , and H_2 . We can further write

$$\dot{\mathbf{x}}_e^t = \dot{R}_1 \hat{\mathbf{x}}_n^e + \dot{R}_2 \hat{\mathbf{x}}_{n+1}^e + \dot{H}_1 \hat{\mathbf{v}}_n^e + \dot{H}_2 \hat{\mathbf{v}}_{n+1}^e, \quad (25)$$

$$\delta \mathbf{x}_e^t = R_1 \delta \hat{\mathbf{x}}_n^e + R_2 \delta \hat{\mathbf{x}}_{n+1}^e + H_1 \delta \hat{\mathbf{v}}_n^e + H_2 \delta \hat{\mathbf{v}}_{n+1}^e, \quad (26)$$

$$\delta \dot{\mathbf{x}}_e^t = \dot{R}_1 \delta \hat{\mathbf{x}}_n^e + \dot{R}_2 \delta \hat{\mathbf{x}}_{n+1}^e + \dot{H}_1 \delta \hat{\mathbf{v}}_n^e + \dot{H}_2 \delta \hat{\mathbf{v}}_{n+1}^e. \quad (27)$$

To improve readability, we will also use the assembled counterparts accounting for all spatial FE nodes at once. We will denote them e.g. by $\hat{\mathbf{x}}_n$ instead of $\hat{\mathbf{x}}_n^e$; see the analogy to $\mathbf{x}(t)$ / $\mathbf{x}_e(t)$ introduced in the previous section.

4.1. Virtual action for a single time interval

The approximation discussed in the previous section is now inserted into the virtual action for a single time interval, $[t_n, t_{n+1}]$; this yields

$$\delta \mathcal{S}_{n+1}^{ht} = \int_{t_n}^{t_{n+1}} \delta L^{ht}(\mathbf{x}^t, \dot{\mathbf{x}}^t) dt, \quad \delta L^{ht}(\mathbf{x}^t, \dot{\mathbf{x}}^t) = (\delta \dot{\mathbf{x}}^t)^T \mathbf{m} \dot{\mathbf{x}}^t - (\delta \mathbf{x}^t)^T \mathbf{f}(\mathbf{x}^t). \quad (28)$$

The increment $\delta \mathcal{S}_{n+1}^{ht}$ depends on four variables: $\hat{\mathbf{x}}_n$, $\hat{\mathbf{x}}_{n+1}$, $\hat{\mathbf{v}}_n$, and $\hat{\mathbf{v}}_{n+1}$; it can thus be reformulated to

$$\delta \mathcal{S}_{n+1}^{ht} = \delta \hat{\mathbf{x}}_n \cdot \frac{\partial \mathcal{S}_{n+1}^{ht}}{\partial \hat{\mathbf{x}}_n} + \delta \hat{\mathbf{x}}_{n+1} \cdot \frac{\partial \mathcal{S}_{n+1}^{ht}}{\partial \hat{\mathbf{x}}_{n+1}} + \delta \hat{\mathbf{v}}_n \cdot \frac{\partial \mathcal{S}_{n+1}^{ht}}{\partial \hat{\mathbf{v}}_n} + \delta \hat{\mathbf{v}}_{n+1} \cdot \frac{\partial \mathcal{S}_{n+1}^{ht}}{\partial \hat{\mathbf{v}}_{n+1}}. \quad (29)$$

Following the notation of Marsden and West [53], we now define the discrete momenta

$$\hat{\mathbf{p}}_n^- := - \frac{\partial \mathcal{S}_{n+1}^{ht}}{\partial \hat{\mathbf{x}}_n}, \quad \hat{\mathbf{p}}_{n+1}^+ := \frac{\partial \mathcal{S}_{n+1}^{ht}}{\partial \hat{\mathbf{x}}_{n+1}}, \quad (30)$$

and two analogous variables coming from the Hermite discretization,

$$\hat{\mathbf{q}}_n^- := - \frac{\partial \mathcal{S}_{n+1}^{ht}}{\partial \hat{\mathbf{v}}_n}, \quad \hat{\mathbf{q}}_{n+1}^+ := \frac{\partial \mathcal{S}_{n+1}^{ht}}{\partial \hat{\mathbf{v}}_{n+1}}. \quad (31)$$

Since $\hat{\mathbf{q}}_n^-$ and $\hat{\mathbf{q}}_{n+1}^+$ have the unit “momentum \times time”, we refer to them as discrete “pseudo-momenta”. The four terms can be computed from the discrete action, \mathcal{S}_{n+1}^{ht} , given in [Appendix A.2](#); this results in

$$\hat{\mathbf{p}}_n^- = - \int_{t_n}^{t_{n+1}} \left[\dot{R}_1(t) \mathbf{m} \dot{\mathbf{x}}^t - R_1(t) \mathbf{f}(\mathbf{x}^t) \right] dt, \quad (32)$$

$$\hat{\mathbf{p}}_{n+1}^+ = \int_{t_n}^{t_{n+1}} \left[\dot{R}_2(t) \mathbf{m} \dot{\mathbf{x}}^t - R_2(t) \mathbf{f}(\mathbf{x}^t) \right] dt, \quad (33)$$

$$\hat{\mathbf{q}}_n^- = - \int_{t_n}^{t_{n+1}} \left[\dot{H}_1(t) \mathbf{m} \dot{\mathbf{x}}^t - H_1(t) \mathbf{f}(\mathbf{x}^t) \right] dt, \quad (34)$$

$$\hat{\mathbf{q}}_{n+1}^+ = \int_{t_n}^{t_{n+1}} \left[\dot{H}_2(t) \mathbf{m} \dot{\mathbf{x}}^t - H_2(t) \mathbf{f}(\mathbf{x}^t) \right] dt. \quad (35)$$

By inserting these (pseudo-)momenta, we can simplify Eq. (29) to

$$\delta \mathcal{S}_{n+1}^{ht} = -\delta \hat{\mathbf{x}}_n \cdot \hat{\mathbf{p}}_n^- + \delta \hat{\mathbf{x}}_{n+1} \cdot \hat{\mathbf{p}}_{n+1}^+ - \delta \hat{\mathbf{v}}_n \cdot \hat{\mathbf{q}}_n^- + \delta \hat{\mathbf{v}}_{n+1} \cdot \hat{\mathbf{q}}_{n+1}^+. \quad (36)$$

In addition, since the variations $\delta \hat{\mathbf{x}}_n$ and $\delta \hat{\mathbf{x}}_{n+1}$ remain arbitrary, $\delta \mathcal{S}_{n+1}^{ht}$ must fulfill Hamilton’s law of varying action applied to the interval $[t_n, t_{n+1}]$,

$$\delta \mathcal{S}_{n+1}^{ht} = \delta \hat{\mathbf{x}}_{n+1} \cdot \mathbf{m} \hat{\mathbf{v}}_{n+1} - \delta \hat{\mathbf{x}}_n \cdot \mathbf{m} \hat{\mathbf{v}}_n. \quad (37)$$

After inserting Eq. (36), we finally obtain the spatially and temporally discrete version of Eq. (12) for a single time interval:

$$\begin{aligned} \delta \hat{\mathbf{x}}_n \cdot \left[\mathbf{m} \hat{\mathbf{v}}_n - \hat{\mathbf{p}}_n^- \right] + \delta \hat{\mathbf{x}}_{n+1} \cdot \left[\hat{\mathbf{p}}_{n+1}^+ - \mathbf{m} \hat{\mathbf{v}}_{n+1} \right] \\ + \delta \hat{\mathbf{v}}_n \cdot \left[-\hat{\mathbf{q}}_n^- \right] + \delta \hat{\mathbf{v}}_{n+1} \cdot \left[\hat{\mathbf{q}}_{n+1}^+ \right] = 0 \quad \forall \delta \hat{\mathbf{x}}_n, \delta \hat{\mathbf{x}}_{n+1}, \delta \hat{\mathbf{v}}_n, \delta \hat{\mathbf{v}}_{n+1}. \end{aligned} \quad (38)$$

Note that we derive Eq. (38) by first varying the continuous action integral, and then discretizing its variation in space and time. We would, however, obtain the same expression if we first discretized the action itself, and then varied the discrete action for a single time interval.

4.2. Solution strategy

In general, variational integrators are constructed by 1) summing up the discrete action for all time intervals, 2) taking its variation, and 3) re-arranging the summands. Doing so for Eq. (38), we would arrive at the following statement:

$$\begin{aligned} \delta \hat{\mathbf{x}}_0 \cdot \left[\mathbf{m} \hat{\mathbf{v}}_0 - \hat{\mathbf{p}}_0^- \right] + \sum_{n=1}^{N-1} \delta \hat{\mathbf{x}}_n \cdot \left[\hat{\mathbf{p}}_n^+ - \hat{\mathbf{p}}_n^- \right] + \delta \hat{\mathbf{x}}_N \cdot \left[\mathbf{m} \hat{\mathbf{v}}_N - \hat{\mathbf{p}}_N^+ \right] \\ + \delta \hat{\mathbf{v}}_0 \cdot \left[-\hat{\mathbf{q}}_0^- \right] + \sum_{n=1}^{N-1} \delta \hat{\mathbf{v}}_n \cdot \left[\hat{\mathbf{q}}_n^+ - \hat{\mathbf{q}}_n^- \right] + \delta \hat{\mathbf{v}}_N \cdot \left[\hat{\mathbf{q}}_N^+ \right] = 0. \end{aligned} \quad (39)$$

This expression is equivalent to Eq. (38) summed up over the entire time domain. Solving Eq. (39) subsequently, however, results in a two-step method that is unconditionally unstable. This phenomenon has also

been investigated by Riff and Baruch [61]. Instead, we develop a class of one-step methods arising from the virtual action for the individual time interval $[t_n, t_{n+1}]$. If the virtual displacements and velocities are presumed to be arbitrary, Eq. (38) provides us with $(4 \cdot d n_{\text{no}})$ equations,

$$\hat{\mathbf{p}}_n^- = \mathbf{m} \hat{\mathbf{v}}_n, \quad (40)$$

$$\hat{\mathbf{p}}_{n+1}^+ = \mathbf{m} \hat{\mathbf{v}}_{n+1}, \quad (41)$$

$$\hat{\mathbf{q}}_n^- = \mathbf{0}, \quad (42)$$

$$\hat{\mathbf{q}}_{n+1}^+ = \mathbf{0}, \quad (43)$$

where n_{no} is the number of finite element nodes. Physically, the first two equations enforce the balance of linear momentum at the boundaries of the current time interval; see Fig. 1. The second two equations arise from the chosen Hermite approach. Assuming that the displacement and velocity of the previous

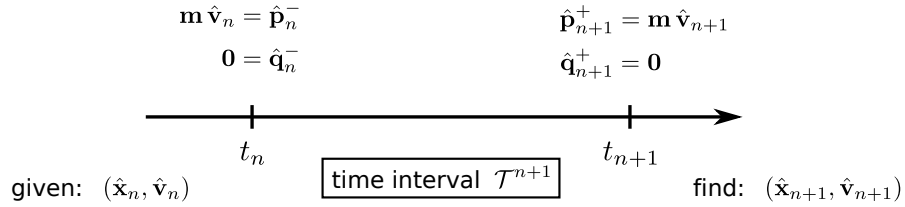


Figure 1: Equilibrium equations for time interval $\mathcal{T}^{n+1} = [t_n, t_{n+1}]$.

time step, $\hat{\mathbf{x}}_n$ and $\hat{\mathbf{v}}_n$, are given, we need only $(2 \cdot d n_{\text{no}})$ equations to determine the new state, $\hat{\mathbf{x}}_{n+1}$ and $\hat{\mathbf{v}}_{n+1}$. The system (40) – (43) is thus over-determined. For this reason, we set two of the (so far arbitrary) variations, $\delta \hat{\mathbf{x}}_n$, $\delta \hat{\mathbf{x}}_{n+1}$, $\delta \hat{\mathbf{v}}_n$, and $\delta \hat{\mathbf{v}}_{n+1}$, to zero; this approach is further motivated in the following. The new deformation and velocity are then computed from the remaining two equations. We finally obtain six methods, which are illustrated in Fig. 2:

pp-scheme

$$\begin{aligned} \delta \hat{\mathbf{v}}_n = \delta \hat{\mathbf{v}}_{n+1} = \mathbf{0} \\ \Rightarrow \quad \hat{\mathbf{p}}_n^- = \mathbf{m} \hat{\mathbf{v}}_n, \quad \hat{\mathbf{p}}_{n+1}^+ = \mathbf{m} \hat{\mathbf{v}}_{n+1}. \end{aligned} \quad (44)$$

This seems to be the most promising approach: From its definition follows that it automatically fulfills conservation of momentum. Here, the velocity is connected to the displacement by setting the physical momenta, $\mathbf{m} \hat{\mathbf{v}}_n$ and $\mathbf{m} \hat{\mathbf{v}}_{n+1}$, equal to the discrete momenta, $\hat{\mathbf{p}}_n^-$ and $\hat{\mathbf{p}}_{n+1}^+$, defined in Eq. (30).

qq-scheme:

$$\begin{aligned} \delta \hat{\mathbf{x}}_n = \delta \hat{\mathbf{x}}_{n+1} = \mathbf{0} \\ \Rightarrow \quad \hat{\mathbf{q}}_n^- = \mathbf{0}, \quad \hat{\mathbf{q}}_{n+1}^+ = \mathbf{0}. \end{aligned} \quad (45)$$

This method can be seen as the counterpart of the pp-scheme.

p⁺q⁻-scheme

$$\begin{aligned} \delta \hat{\mathbf{x}}_n = \delta \hat{\mathbf{v}}_{n+1} = \mathbf{0} \\ \Rightarrow \quad \hat{\mathbf{p}}_{n+1}^+ = \mathbf{m} \hat{\mathbf{v}}_{n+1}, \quad \hat{\mathbf{q}}_n^- = \mathbf{0}. \end{aligned} \tag{46}$$

This is one of four mixed methods, varying once the displacement and once the velocity.

p⁺q⁺-scheme

$$\begin{aligned} \delta \hat{\mathbf{x}}_n = \delta \hat{\mathbf{v}}_n = \mathbf{0} \\ \Rightarrow \quad \hat{\mathbf{p}}_{n+1}^+ = \mathbf{m} \hat{\mathbf{v}}_{n+1}, \quad \hat{\mathbf{q}}_{n+1}^+ = \mathbf{0}. \end{aligned} \tag{47}$$

This scheme corresponds to the formulation proposed by G eradin [22].

p⁻q⁻-scheme

$$\begin{aligned} \delta \hat{\mathbf{x}}_{n+1} = \delta \hat{\mathbf{v}}_{n+1} = \mathbf{0} \\ \Rightarrow \quad \hat{\mathbf{p}}_n^- = \mathbf{m} \hat{\mathbf{v}}_n, \quad \hat{\mathbf{q}}_n^- = \mathbf{0}. \end{aligned} \tag{48}$$

p⁻q⁺-scheme

$$\begin{aligned} \delta \hat{\mathbf{x}}_{n+1} = \delta \hat{\mathbf{v}}_n = \mathbf{0} \\ \Rightarrow \quad \hat{\mathbf{p}}_n^- = \mathbf{m} \hat{\mathbf{v}}_n, \quad \hat{\mathbf{q}}_{n+1}^+ = \mathbf{0}. \end{aligned} \tag{49}$$

Interestingly, the resulting six methods have completely different characteristics; it is not surprising that some of them are more favorable than others. In Section 5, we investigate the characteristics of each scheme in terms of stability, symplecticity, and preservation of energy. For several reasons we especially focus on the first two schemes: pp and qq. First, from the definition of the pp-scheme (44) directly follows that the two discrete momenta, $\hat{\mathbf{p}}_n^+$ and $\hat{\mathbf{p}}_n^-$, must be equal to each other. Therefore, the discrete Euler-Lagrange equations, $\hat{\mathbf{p}}_n^+ - \hat{\mathbf{p}}_n^- = \mathbf{0}$, are fulfilled automatically (cf. Chapter VI, Eq. (6.7) of Hairer et al. [25]). The two velocities, $\hat{\mathbf{v}}_n$ and $\hat{\mathbf{v}}_{n+1}$, are finally connected to the displacements, $\hat{\mathbf{x}}_n$ and $\hat{\mathbf{x}}_{n+1}$, by setting the physical momenta, $\mathbf{m} \hat{\mathbf{v}}_n$ and $\mathbf{m} \hat{\mathbf{v}}_{n+1}$, equal to the discrete momenta. Note that this approach would not be possible for integration methods with the usual C^0 -continuous approximations for the displacement at the discrete time steps.

Nevertheless, we must point out that our six integrators are not variational; this becomes apparent especially for the four mixed methods, where we use one zero-variation for the displacement, and one for the velocity. The pp- and qq-scheme, however, are consistently derived from Hamilton's law in the sense that they consider, at a certain time step t_n , the same zero-variations for both the preceding and succeeding

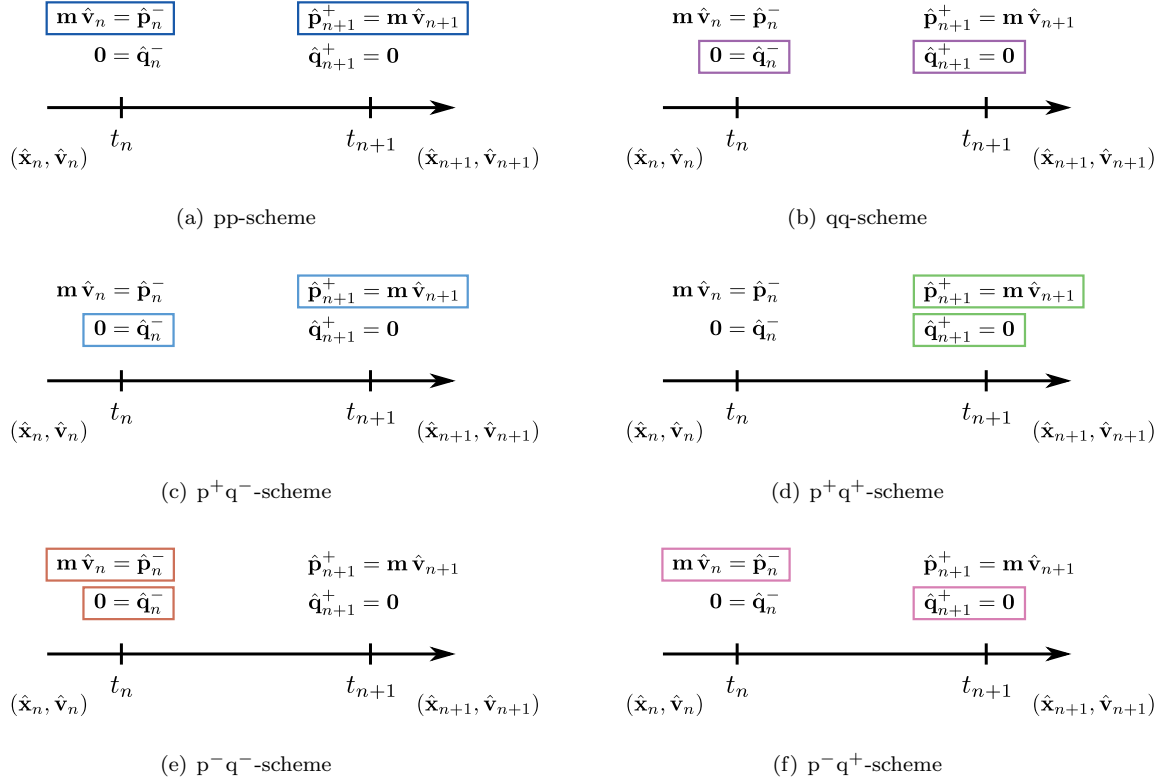


Figure 2: Illustration of the six integration schemes.

time intervals: $[t_{n-1}, t_n]$ and $[t_n, t_{n+1}]$. We further show in the following that — at least for simple linear problems — the first two methods (44) and (45) have similar properties like variational integrators, such as symplecticity. In addition, we numerically demonstrate that these methods show a very good energy-preserving behavior even for nonlinear problems with multiple degrees of freedom. In future work, it would be thus interesting to investigate symplecticity for arbitrary systems.

4.3. Implementation

In general, the set of equations (40) – (43) is nonlinear. It thus must be linearized by using e.g. Newton's method; this provides us with a linear system of equations that is iteratively solved for the new positions and velocities of the finite element nodes. For the linearization, the derivatives of the discrete (pseudo-)momenta are required; these are given in Appendix A.3. In analogy to the force vectors and the mass matrix, the terms $\hat{\mathbf{p}}_n^-$, $\hat{\mathbf{p}}_{n+1}^+$, $\hat{\mathbf{q}}_n^-$, and $\hat{\mathbf{q}}_{n+1}^+$ can be computed by assembling the contributions of each spatial element, denoted by $\hat{\mathbf{p}}_{e,n}^-$, $\hat{\mathbf{p}}_{e,n+1}^+$, $\hat{\mathbf{q}}_{e,n}^-$, and $\hat{\mathbf{q}}_{e,n+1}^+$. Where possible, the integrals should be computed analytically; this can be done for the contributions due to 1) the kinetic energy and due to 2) any linear elastic internal energy (Appendix A.4). The remaining integrals are approximated by Gaussian quadrature, choosing a sufficient number of quadrature points. For our time integration schemes, neither the kinetic/potential

energy nor the total energy of the system must be evaluated explicitly. Nevertheless, since we want to investigate them in our numerical examples, we summarize these quantities in [Appendix A.2](#).

4.4. Relation to other methods

The idea of applying Hamilton’s law of varying action to initial value problems in structural dynamics goes back to the first approaches using finite elements in both space and time; see e.g. Argyris and Scharpf [1], Fried [19], and Bailey [2]. In contrast to Hamilton’s principle (where the displacement is kept fixed at $t = 0$ and $t = T$) this law incorporates zero-variations for both the initial displacement and the initial velocity: $\delta\mathbf{x}(0) = \delta\mathbf{v}(0) = \mathbf{0}$.

This idea has motivated Baruch and Riff [6] to combine different zero-variations of either the displacement or velocity at both $t = 0$ and $t = T$. Their approach results in six different methods that can be related — with several important differences — to our schemes. Since the same authors have discovered in a previous work [61] the instability of the solution scheme given by Eq. (39), they propose a modified discretization of the virtual displacements in Ref. [62]. In their approach, $\delta\mathbf{x}^t(t)$ is discretized by considering the second derivatives of the shape functions, $\ddot{R}_\bullet(t)$ and $\ddot{H}_\bullet(t)$; the variation of the displacement is thus approximated by a linear (instead of a cubic) function in time. This modification leads to different partial derivatives of the action, and therefore to a different integration method. An even more important difference to our schemes concerns the zero-variations at the boundaries: While Riff and Baruch [62] consider the boundaries of the entire time domain ($t = 0$ and $t = T$), we derive our schemes from zero-variations within each time interval, $[t_n, t_{n+1}]$. Our approach results in six different one-step methods solving the equations subsequently. In contrast, this is possible only for the so-called F4-method of Ref. [62], where $\delta\mathbf{x}(T) = \delta\mathbf{v}(T) = \mathbf{0}$. For the remaining formulations in Ref. [62], all equations would have to be solved simultaneously. In summary, one could loosely relate our six schemes to a subsequent application of the methods by Riff and Baruch [62] for each time interval, $[t_n, t_{n+1}]$. The underlying equations, however, are approximated differently. Besides that, the references mentioned above discuss only linear dynamic systems (where the forces depend on the displacement linearly). Properties like symplecticity and conservation of momentum are not investigated in these studies.

Recently, Leok and Shingel [45] have proposed a variational integrator based on Hermite finite elements in time. Their formulation is derived from a prolongation-collocation approach: In addition to the discrete Euler-Lagrange equations this method accounts for the system’s equation of motion in strong form,

$$\mathbf{m}\ddot{\mathbf{x}}^t(t_\bullet) + \mathbf{f}[\mathbf{x}^t(t_\bullet)] = \mathbf{0}, \quad \bullet = \{n, n + 1\}. \quad (50)$$

For cubic Hermite shape functions — as they are used in our schemes — the velocities, $\hat{\mathbf{v}}_n$ and $\hat{\mathbf{v}}_{n+1}$, are computed from Eq. (50), using

$$\ddot{\mathbf{x}}^t(t) = \ddot{R}_1(t)\hat{\mathbf{x}}_n + \ddot{R}_2(t)\hat{\mathbf{x}}_{n+1} + \ddot{H}_1(t)\hat{\mathbf{v}}_n + \ddot{H}_2(t)\hat{\mathbf{v}}_{n+1}; \quad (51)$$

cf. Eq. (25). These expressions are inserted into the temporally discrete action for one time interval, \mathcal{S}_{n+1}^t , which then depends only on the displacements, $\hat{\mathbf{x}}_n$ and $\hat{\mathbf{x}}_{n+1}$. The final time integration method of Leok and Shingel is obtained by 1) varying the incremental action, \mathcal{S}_{n+1}^t , with respect to the displacements, and 2) setting the total virtual action to zero. Compared to our six Hermite formulations, the resulting method requires only half the number of unknowns to be solved within each time step. Its rate of convergence, however, is lower than the best of our schemes; see Section 5.4. Note that the combination of both spatial and temporal discretizations is not discussed in Ref. [45].

5. Properties of the six schemes

We now investigate the different properties of the six formulations, first focusing on a linear problem with a single degree of freedom. Section 5.1 studies the long-term behavior of the schemes for a simple harmonic oscillator. For this mechanical system the stability properties are discussed in Section 5.2. Section 5.3 investigates the symplecticity of two schemes (pp and qq) for the harmonic oscillator. The convergence behavior is finally analyzed in Section 5.4.

5.1. Long-term behavior

Consider a simple harmonic oscillator, i.e. a spring pendulum with mass m and stiffness k . For an initial elongation of $u_0 = u(0)$, the displacement and velocity of the oscillator can be computed analytically: $u_{\text{an}}(t) = u_0 \cos(\omega t)$ and $v_{\text{an}}(t) = -\omega u_0 \sin(\omega t)$. The frequency of oscillation is given by $\omega = \sqrt{k/m}$; the period length (i.e. the duration of one oscillation) is determined through $T_0 = 2\pi/\omega$. In the following, the numerical results are normalized by u_0 , ω , T_0 , and by the initial energy of the system, $E_0 = \frac{1}{2} k u_0^2$.

We now compare our Hermite schemes with the implicit Newmark algorithm [55], choosing the Newmark parameters as $\beta = 1/4$ and $\gamma = 1/2$. Regarding linear systems, this method is then not only unconditionally stable; it can further conserve the energy (see e.g. Ref. [32] or [41]). Besides, it is shown in Ref. [39] that for $\gamma = 1/2$, the Newmark is variational. In addition to the Newmark algorithm, we consider a variational integrator based on linear finite elements in time (see Appendix B). We will refer to this method as L1-integrator.

Fig. 3 shows the displacement and the velocity of the oscillator for three periods and a very coarse time discretization. As expected, for our six schemes the displacement (velocity) is C^1 -continuous (C^0 -continuous) at the discrete time steps. In contrast, the L1-integrator approximates the velocity as a constant along each time interval; this leads to discontinuities at the interval boundaries. Note that for the Newmark algorithm, the displacement and velocity can be evaluated only at the discrete time steps, t_n . We further observe that the oscillation period increases for both Newmark's method and the L1-integrator.

Regarding the maximum displacement, for two of our mixed methods (p^-q^+ and p^-q^-) the amplitude of oscillation seems to increase strongly (Fig. 3(a)). This indicates that these methods may be unstable.

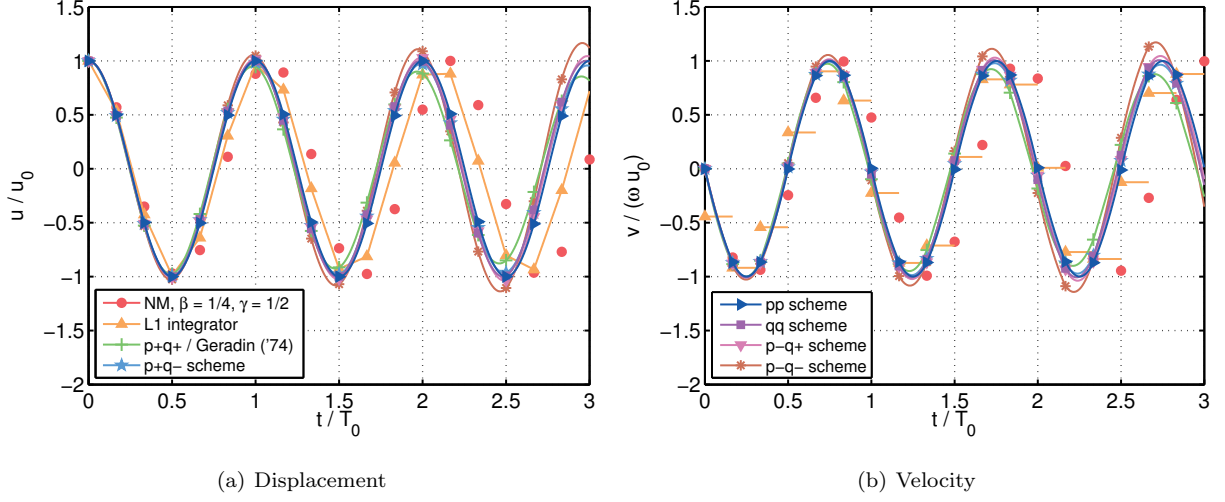


Figure 3: Harmonic oscillator: Displacement and velocity for three periods of oscillation; the six Hermite schemes are compared with the Newmark algorithm (NM) and with the L1-integrator; $\Delta t = T_0/6$.

For the remaining mixed schemes (p^+q^+ /Gérardin and p^+q^-) the amplitudes in both the displacement and velocity decrease. In contrast, both the amplitude and the period of oscillation are well-preserved for our pp- and qq-schemes.

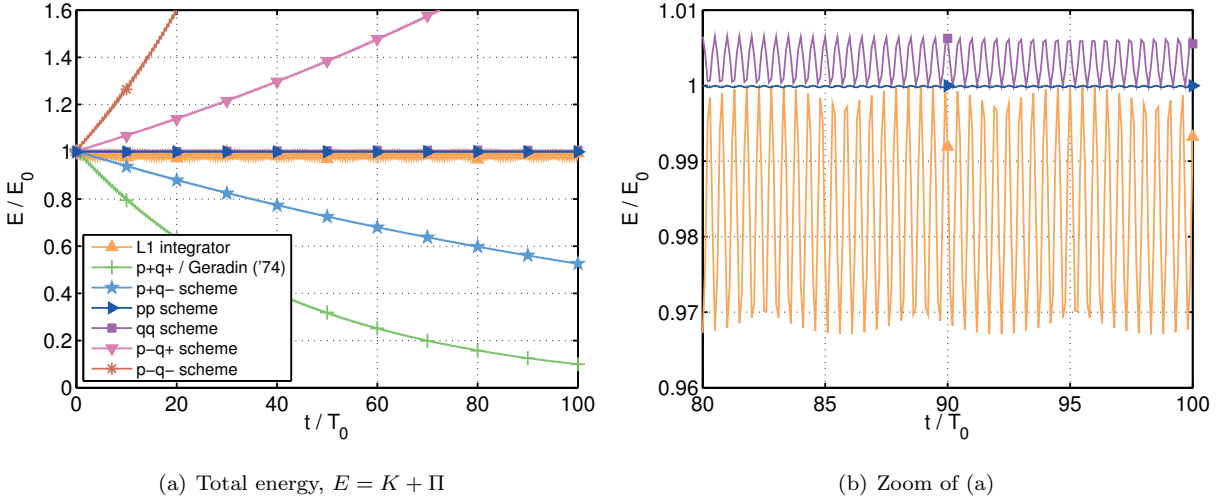


Figure 4: Harmonic oscillator: Long-term energy behavior for 100 periods of oscillation; the six Hermite schemes are compared with the L1-integrator; $\Delta t = T_0/10$.

Fig. 4 shows the total energy of the system over 100 oscillation periods. The maximum relative error observed for the time domain $[0, T]$ is given in Table 1. Both the figures and the table show that the schemes p^-q^+ and p^-q^- are unstable, while the schemes p^+q^+ and p^+q^- are strongly dissipative. This agrees with the results shown in Fig. 3. As expected, for both the remaining two schemes, pp and qq, and

for the L1-integrator, the total energy is qualitatively preserved. Interestingly, the pp- and the qq-scheme are more accurate; this is indicated by smaller amplitudes of oscillation in Fig. 4(b). Compared to the linear integrator, the maximum relative errors are smaller by one order of magnitude for the qq-scheme, and even two orders for the pp-scheme.

	pp	qq	p ⁺ q ⁻	p ⁺ q ⁺	p ⁻ q ⁻	p ⁻ q ⁺	L1
e_E^{\max}	0.023 %	0.653 %	47.51 %	90.08 %	918.6 %	91.58 %	3.29 %

Table 1: Harmonic oscillator: Maximum error in the total energy at the discrete time steps, $e_E^{\max} := \max |E(t_n) - E_0| / E_0$, $n = 0, \dots, N$; $T = 100 T_0$, $\Delta t = T_0/10$.

5.2. Stability

Following Leimkuhler and Reich [44] and Ober-Blöbaum and Saake [57], we now investigate the stability of the six schemes by means of the harmonic oscillator. For this purpose, we introduce the normalized time step $\gamma := \omega \Delta t$ and insert it into Eq. (44) – (49). Then the six schemes can be expressed in the form

$$\begin{bmatrix} v_{n+1} \\ \omega u_{n+1} \end{bmatrix} = \mathbf{A} \begin{bmatrix} v_n \\ \omega u_n \end{bmatrix}, \quad (52)$$

where \mathbf{A} is the amplification matrix given in Appendix C. The terms u_n and v_n denote the displacement and the velocity at time step t_n . Fig. 5 shows the spectral radius for each of the schemes, defined by

$$\rho(\mathbf{A}) := \max(|\lambda_1|, |\lambda_2|), \quad \det(\mathbf{A} - \lambda_i \mathbf{I}_2) = 0, \quad i = 1, 2. \quad (53)$$

Table 2 shows the maximum permitted time step, Δt_{stab} , for which the schemes are stable, i.e. for which $\rho(\mathbf{A}) \leq 1$. Both the table and Fig. 5(b) show that the last two schemes, p⁻q⁻ and p⁻q⁺, are unstable even for very small time steps. In contrast, the schemes p⁺q⁻ and p⁺q⁺ seem to be stable for large time steps; nevertheless, these methods are numerically dissipative because of $\rho(\mathbf{A}) < 1$ for $\gamma < \gamma_{\text{stab}}$ (see Fig. 5(b)). The most promising methods seem to be the pp-scheme and the qq-scheme; they show both excellent stability and energy preservation.

	pp	qq	p ⁺ q ⁻	p ⁺ q ⁺	p ⁻ q ⁻	p ⁻ q ⁺
$\gamma_{\text{stab}} [-]$	3.144	3.055	3.083	9.165	$8.24 \cdot 10^{-4}$	$6.04 \cdot 10^{-4}$
$\Delta t_{\text{stab}} [T_0]$	0.500	0.486	0.491	1.459	$1.31 \cdot 10^{-4}$	$9.61 \cdot 10^{-5}$

Table 2: Harmonic oscillator: Maximum time steps, γ_{stab} and Δt_{stab} , for which the schemes are stable, i.e. $\rho(\mathbf{A}) \leq 1 + 10^{-15}$.

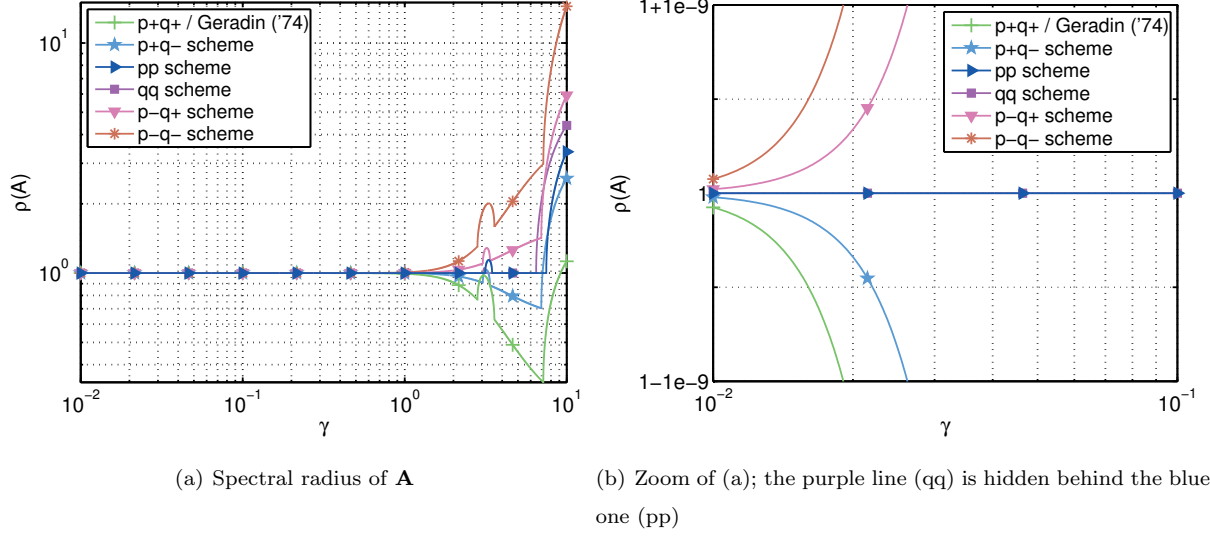


Figure 5: Harmonic oscillator: Spectral radius for the six Hermite schemes as a function of the normalized time step, γ .

5.3. Symplecticity

As discussed in Section 5.1, both the pp-scheme and the qq-scheme preserve — at least for the linear oscillator — the energy of the system well. This motivates us to investigate whether these methods are generally symplectic. We focus here on simple linear systems; in particular, we investigate symplecticity by means of the harmonic oscillator. One way to prove symplecticity is to investigate the derivatives of the phase state, $(\hat{\mathbf{p}}_{n+1}, \hat{\mathbf{x}}_{n+1})$, w.r.t. the previous state, $(\hat{\mathbf{p}}_n, \hat{\mathbf{x}}_n)$. Here, $\hat{\mathbf{p}}_\bullet$ is the physical momentum, which can be computed from the velocity by $\hat{\mathbf{p}}_\bullet = \mathbf{m} \hat{\mathbf{v}}_\bullet$. This results in the Jacobian

$$\mathbf{B}_{n+1} := \begin{bmatrix} \frac{\partial \hat{\mathbf{p}}_{n+1}}{\partial \hat{\mathbf{p}}_n} & \frac{\partial \hat{\mathbf{p}}_{n+1}}{\partial \hat{\mathbf{x}}_n} \\ \frac{\partial \hat{\mathbf{x}}_{n+1}}{\partial \hat{\mathbf{p}}_n} & \frac{\partial \hat{\mathbf{x}}_{n+1}}{\partial \hat{\mathbf{x}}_n} \end{bmatrix} = \begin{bmatrix} \mathbf{m} \frac{\partial \hat{\mathbf{v}}_{n+1}}{\partial \hat{\mathbf{v}}_n} \mathbf{m}^{-1} & \mathbf{m} \frac{\partial \hat{\mathbf{v}}_{n+1}}{\partial \hat{\mathbf{x}}_n} \\ \frac{\partial \hat{\mathbf{x}}_{n+1}}{\partial \hat{\mathbf{v}}_n} \mathbf{m}^{-1} & \frac{\partial \hat{\mathbf{x}}_{n+1}}{\partial \hat{\mathbf{x}}_n} \end{bmatrix}. \quad (54)$$

According to Ref. [25], the mapping $(\hat{\mathbf{p}}_n, \hat{\mathbf{x}}_n) \mapsto (\hat{\mathbf{p}}_{n+1}, \hat{\mathbf{x}}_{n+1})$ is symplectic if \mathbf{B}_{n+1} is symplectic, i.e. if

$$\mathbf{B}_{n+1}^T \mathbf{J} \mathbf{B}_{n+1} = \mathbf{J}, \quad \mathbf{J} = \begin{bmatrix} \mathbf{0} & \mathbf{I}_{d \cdot n_{\text{no}}} \\ -\mathbf{I}_{d \cdot n_{\text{no}}} & \mathbf{0} \end{bmatrix}, \quad n = 0, \dots, N-1, \quad (55)$$

where $\mathbf{I}_{d \cdot n_{\text{no}}}$ is the identity matrix of dimension $d \cdot n_{\text{no}}$. For the harmonic oscillator, the Jacobian reduces to

$$\mathbf{B}_{n+1} = \begin{bmatrix} \frac{\partial v_{n+1}}{\partial v_n} & m \frac{\partial v_{n+1}}{\partial u_n} \\ \frac{1}{m} \frac{\partial u_{n+1}}{\partial v_n} & \frac{\partial u_{n+1}}{\partial u_n} \end{bmatrix}. \quad (56)$$

In this case one can show that the determinant of \mathbf{B}_{n+1} is equal to the determinant of the amplification matrix introduced in Eq. (52): $\det(\mathbf{B}_{n+1}) = \det(\mathbf{A})$. With this relation the condition for symplecticity (55) is fulfilled if the determinant of \mathbf{A} is equal to one,

$$\begin{bmatrix} 0 & \det(\mathbf{A}) \\ -\det(\mathbf{A}) & 0 \end{bmatrix} = \begin{bmatrix} 0 & 1 \\ -1 & 0 \end{bmatrix} \quad \Rightarrow \quad \det(\mathbf{A}) = 1. \quad (57)$$

From Appendix C we obtain

$$\det(\mathbf{A}_{\text{pp}}) = 1, \quad \det(\mathbf{A}_{\text{qq}}) = 1 \quad \forall \gamma. \quad (58)$$

We thus have shown that — at least for the harmonic oscillator — both our pp-scheme and qq-scheme are symplectic. It remains to be subject of further investigation whether this is also true for arbitrary systems with multiple degrees of freedom.

5.4. Convergence behavior

We now focus on the four stable schemes: pp, qq, p^+q^- , and p^+q^+ (which is equivalent to the method of G eradin [22]). In order to study convergence for the harmonic oscillator we consider the maximum errors of the displacement, velocity, and total energy at the discrete time steps; these are given by

$$e_{\bullet}^{\max} = \max_{n=0,\dots,N} |e_{\bullet}(t_n)|, \quad \bullet = \{u, v, E\}, \quad (59)$$

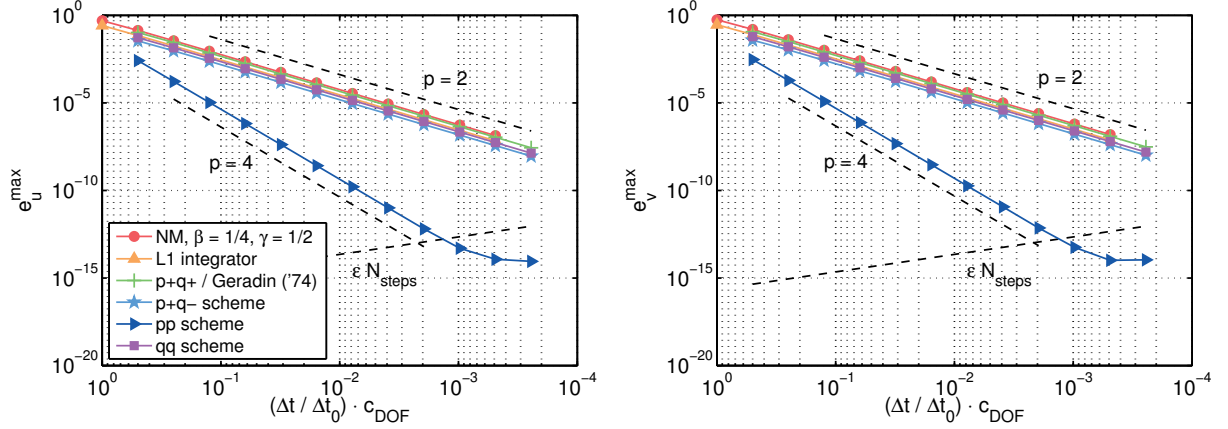
where

$$e_u(t) = |u(t) - u_{\text{an}}(t)| / |u_0|, \quad e_v(t) = |v(t) - v_{\text{an}}(t)| / |\omega u_0|, \quad e_E(t) = |E(t) - E_0| / E_0. \quad (60)$$

Fig. 6 shows the convergence behavior of these errors for our stable schemes, the Newmark algorithm, and the L1-integrator. In addition, we account for the results discussed by Leok and Shingel [45] for cubic Hermite interpolation. Note that compared to the last three methods, our time integration schemes must account for twice the number of unknowns in each step: The nodal displacements and the nodal velocities. This has been considered in the scaling of the abscissae by introducing the factor c_{DOF} ($c_{\text{DOF}} = 1/2$ for our schemes, otherwise $c_{\text{DOF}} = 1$).

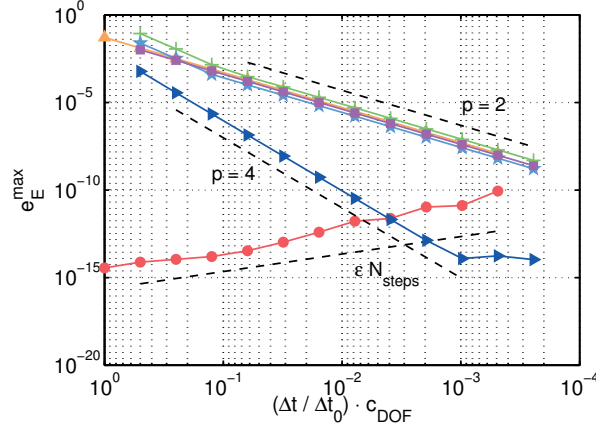
As already shown in Fig. 3(b), for the L1-integrator the piecewise approximation of the velocity is discontinuous at the discrete time steps. Nevertheless, we can determine the physical velocity at t_n by computing the momentum from a discrete Legendre transformation [25]. This approach is also discussed by Ober-Bl obaum et al. [56] considering boundary conditions for the velocity. For the L1-integrator the maximum errors in both the velocity and in the energy (Fig. 6(b) and 6(c)) are finally obtained by using

$$\hat{\mathbf{v}}_n = \mathbf{m}^{-1} \hat{\mathbf{p}}_n, \quad \hat{\mathbf{p}}_n := -\frac{\partial \mathcal{S}_{n+1}^{ht}(\hat{\mathbf{x}}_n, \hat{\mathbf{x}}_{n+1})}{\partial \hat{\mathbf{x}}_n} = \frac{\partial \mathcal{S}_n^{ht}(\hat{\mathbf{x}}_{n-1}, \hat{\mathbf{x}}_n)}{\partial \hat{\mathbf{x}}_n}. \quad (61)$$



(a) Max. error in the displacement for t_0, \dots, t_N

(b) Max. error in the velocity for t_0, \dots, t_N



(c) Max. error in the energy for t_0, \dots, t_N

Figure 6: Harmonic oscillator: Convergence behavior for $T = 2T_0$, $\Delta t_0 = T_0/8$; $c_{\text{DOF}} = 1/2$ for our Hermite schemes, otherwise $c_{\text{DOF}} = 1$; the dashed line labeled with $\varepsilon N_{\text{steps}}$ indicates the estimated machine precision multiplied with the number of computed steps.

As expected, Newmark's method can conserve the energy of the system; the corresponding error thus lies in the range of machine precision. The errors in the displacement and in the velocity, however, are of order $p = 2$. The same rate of convergence can be observed for the L1-integrator. This agrees with the discussion in Ref. [57] that integrators interpolating the displacement linearly in time can be at most of second order.

Our schemes p^+q^+ , p^+q^- , and qq (including the formulation by G eradin [22]) also show an order of $p = 2$. Since their computational effort is higher than for both Newmark's method and the L1-integrator, these methods are not favorable. In comparison, Leok and Shingel prove convergence with order three for their integrator based on cubic Hermite interpolation (i.e. $n = 2$ in Theorem 2 of Ref. [45]). An even better

rate of convergence is achieved for our favorite candidate, the pp-scheme: At the discrete time steps, the errors in 1) the displacement, 2) the velocity, and 3) the energy converge with order $p = 4$.

6. Numerical results for 1D elastodynamics

The previous sections have shown that our pp-scheme is symplectic for the harmonic oscillator; it further possess the highest rate of convergence. So far only linear problems with a single degree of freedom have been studied. For this reason, the following section discusses the application of the pp-scheme to spatially continuous bodies. Section 6.1 investigates the free axial vibration of a linear elastic bar. Here, the error with respect to the analytical solution is discussed for different types of spatial elements. Section 6.2 discusses the axial deformation of a bar exhibiting a nonlinear material behavior.

6.1. Axial vibration of a linear elastic bar

We now consider the free axial vibration of a linear elastic bar (Appendix D). For the spatial discretization we use either linear Lagrange or cubic Hermite finite elements; see Appendix A.1 and text books such as Ref. [71]. The second kind of element yields a C^1 -continuous approximation of the displacement also in space.

6.1.1. Vibration in the first eigenmode

The first example shown here governs the bar vibrating in the first (i.e. the lowest) characteristic eigenmode. For this test case, the corresponding displacement, velocity, and energy can be analytically computed from the one-dimensional wave equation; this yields

$$u_{\text{an}}(X, t) = u_0 \cdot \cos\left(\frac{\pi X}{L}\right) \cdot \cos(\omega_{\text{an}} t), \quad v_{\text{an}}(X, t) = -u_0 \cdot \cos\left(\frac{\pi X}{L}\right) \cdot \omega_{\text{an}} \sin(\omega_{\text{an}} t), \quad (62)$$

where $X \in [0, L]$, and

$$E_0 = \frac{EA}{4L} (\pi u_0)^2. \quad (63)$$

Here, u_0 is the amplitude of oscillation, and ω_{an} is the first natural frequency, given by $\omega_{\text{an}} = \pi \sqrt{E/(\rho_0 L^2)}$. The deformation of the bar vibrating in the first mode is shown in Fig. 7. Here, six linear elements are used for the spatial discretization. As expected, the bar performs sinusoidal oscillations. Due to the coarse finite element mesh, however, the structure oscillates with a frequency slightly higher than the analytical solution: $|\omega - \omega_{\text{an}}|/\omega_{\text{an}} \approx 1.15\%$. This implies that the oscillation period of the discrete system, T_0 , is smaller than the analytical solution, $T_0^{\text{an}} = 2\pi/\omega_{\text{an}}$.

Note that the size of the time step, Δt , has to fit to the considered spatial FE element mesh. Since a stability analysis including spatial discretization can be quite tedious, we roughly estimate the maximum

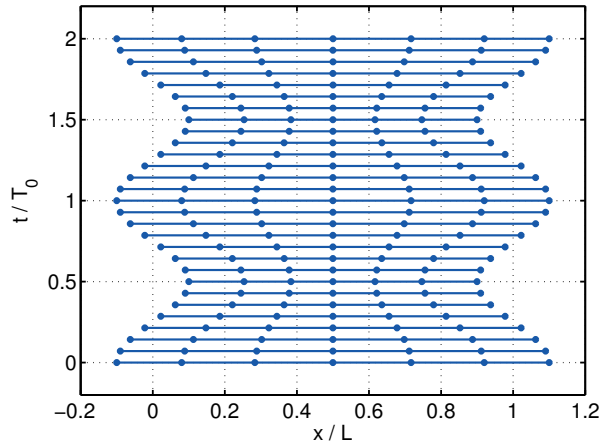


Figure 7: Linear elastic bar: Deformation for two oscillations in the first natural frequency using the pp-scheme and linear FE; $\Delta t = T_0/14$, $L_e = L/6$.

permitted time step for either linear or Hermite elements. We therefore consider the Courant-Friedrichs-Lewy (CFL) condition for one-dimensional problems,

$$C_{\text{CFL}} \leq C^{\text{max}}, \quad C_{\text{CFL}} := \frac{c_{\text{W}} \cdot \Delta t}{\Delta L}, \quad (64)$$

where $c_{\text{W}} = \sqrt{E/\rho_0}$ is the velocity of wave propagation, and ΔL is the characteristic discretization length. For a linearly interpolated element applies $\Delta L := L_e$; for a Hermite finite element, we choose $\Delta L := L_e/2$ to take into account that it has twice the number of unknowns (and thus higher accuracy).

We now vary the CFL number for a bar vibrating for at least 1000 oscillations. The estimated maximum values are useful to choose appropriate parameters for the following numerical examples. Of course we cannot ensure, however, stability for arbitrary CFL numbers smaller than these estimates. As shown in the stability analysis for a single degree of freedom (Sect. 5.2), the methods may also become unstable for small ranges of parameters. This becomes apparent in Fig. 5(a), where the spectral radius of the pp-scheme exceeds the limit (one) for a small range of time steps, while being stable again for larger steps. Apart from that, the CFL condition does not serve as sufficient condition for stability.

For linear finite elements we estimate $C_{\text{LI}}^{\text{max}} \approx 1.00$ and $C_{\text{pp}}^{\text{max}} \approx 0.90$; this implies that the time step should fulfill $\Delta t \leq 1.00 \Delta L/c_{\text{W}}$ for the L1-integrator, and $\Delta t \leq 0.90 \Delta L/c_{\text{W}}$ for the pp-scheme. For Hermite finite elements we obtain $C_{\text{LI}}^{\text{max}} \approx 0.72$ and $C_{\text{pp}}^{\text{max}} \approx 0.96$. Note that for linear problems Newmark's method is unconditionally stable if $\beta = 1/4$ and $\gamma = 1/2$.

6.1.2. Convergence for the bar

Reconsider the first axial vibration discussed in the previous section. Following Demoures et al. [17], we introduce for the displacement and velocity discrete L^2 -norms that take into account the relative errors at

all time steps and finite element nodes:

$$\|e_{\bullet}\|_{\Sigma} := \sqrt{\sum_{n=0}^N \sum_{I=1}^{n_{\text{no}}} \frac{|e_{\bullet}(X_I, t_n)|^2}{(N+1) \cdot n_{\text{no}}}}, \quad \bullet = \{u, v\}. \quad (65)$$

This corresponds to the Frobenius norm of the arrays $e_u(X_I, t_n)$ and $e_v(X_I, t_n)$ normalized by (the square roots of) the numbers of nodes and time steps. The relative errors are defined as

$$e_u(X, t) = |u(X, t) - u_{\text{an}}(X, t)| / |u_0|, \quad e_v(X, t) = |v(X, t) - v_{\text{an}}(X, t)| / |\omega_{\text{an}} u_0|. \quad (66)$$

In analogy to Eq. (65), we define a discrete L^2 -norm for the error in the energy,

$$\|e_E\|_{\Sigma} := \sqrt{\sum_{n=0}^N \frac{|e_E(t_n)|^2}{N+1}}, \quad (67)$$

using $e_E(t)$ from Eq. (60). Fig. 8 shows the convergence behavior of the displacement and the velocity for the bar discretized either by linear and Hermite elements; Fig. 9 shows the convergence of the error in the total energy. Here, we consider two fixed CFL numbers, while refining both the mesh and the time step simultaneously. Our pp-scheme is finally compared with the L1-integrator and with the Newmark algorithm.

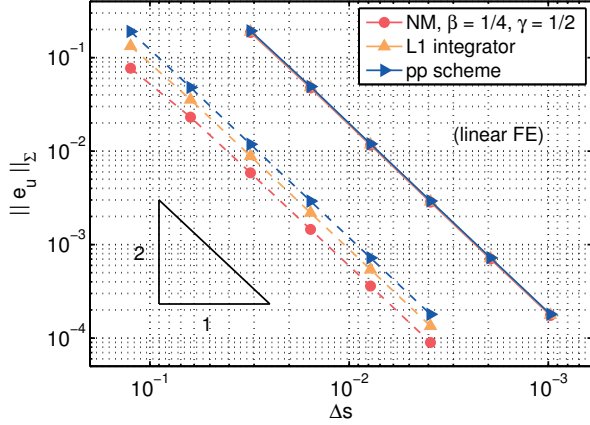
For a linear finite element mesh (i.e. for the left columns of Fig. 8 and 9), the three time discretization methods converge with the same order. This indicates that for this specific problem, the error caused by the spatial discretization predominates. We assume that this is mainly caused by the spatial discretization error in the frequency of vibration. In contrast, the error due to the spatial Hermite discretization carries considerably less weight. The pp-scheme yields a significantly higher convergence than for both the Newmark algorithm and the L1-integrator.

Note that if the bar is discretized by using n_{el} linear elements, the resulting system can be treated as a naturally discrete spring-mass system consisting of n_{el} springs. For such a spring-mass system, the (temporally) analytical solution is given by

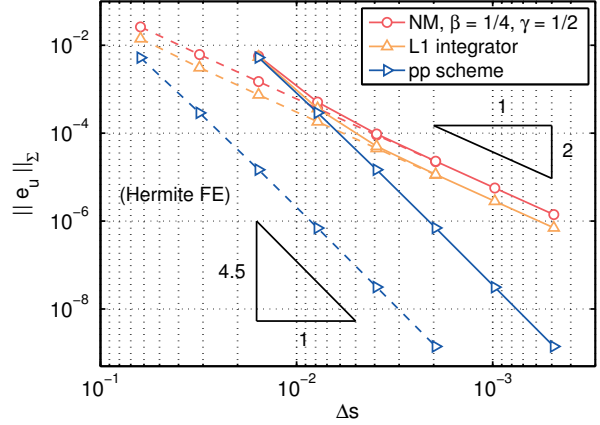
$$u_{\text{an}}^h(X_I, t) = u_0 \cdot \cos\left(\frac{\pi X_I}{L}\right) \cdot \cos(\omega t), \quad v_{\text{an}}^h(X_I, t) = -u_0 \cdot \cos\left(\frac{\pi X_I}{L}\right) \cdot \omega \sin(\omega t), \quad I = 1, \dots, n_{\text{no}}; \quad (68)$$

cf. Eq. (62). The natural frequency, ω , can be determined by analyzing the eigenmodes of the discrete system. Fig. 10(a) and 10(b) show the maximum errors in the displacement and velocity arising from the temporal discretization. Here, the errors e_u^h and e_v^h are determined from Eq. (66), inserting the analytical solutions given by Eq. (68). As expected, the orders of convergence agree with those studied for a single degree of freedom (Section 5.4).

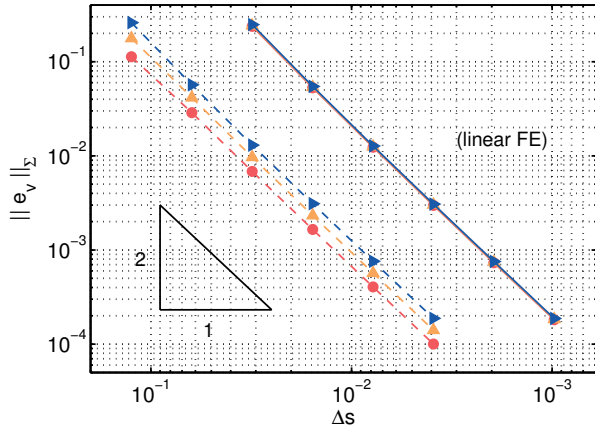
Table 3 compares the computational cost of the three methods for those results shown in the right column of Fig. 8, $C_{\text{CFL}} = 0.5$. Therefore, we measure the computation time that is required to obtain an



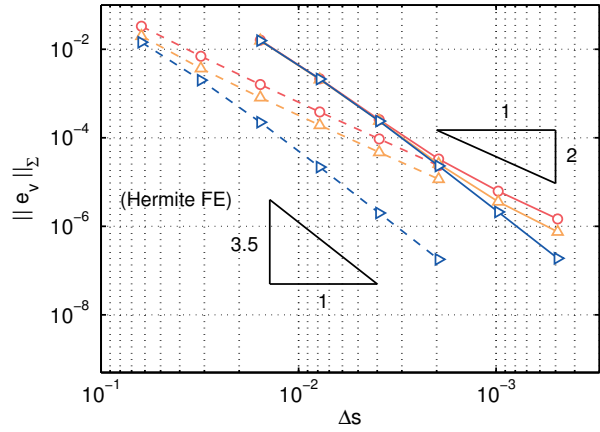
(a) Error in the displacement for spatially linear FE



(b) Error in the displacement for spatial Hermite FE



(c) Error in the velocity for spatially linear FE



(d) Error in the velocity for spatial Hermite FE

Figure 8: Linear elastic bar: Convergence behavior of the displacement and the velocity refining both the mesh and time step; the parameter Δs is given by $\Delta s = \Delta t / T_0^{\text{an}} = C_{\text{CFL}} \cdot \Delta L / (2L)$; shown are $C_{\text{CFL}} = 0.5$ (dashed line) $C_{\text{CFL}} = 0.125$ (solid line) for $T = 1 T_0^{\text{an}}$.

error in the displacement, $\|e_u\|_{\Sigma}$, smaller than 1%, 0.1%, or 0.01%; see Fig. 8(b). Although the pp-scheme must account for twice the number of unknowns within each time step, it takes — due to its higher order of convergence — less computation time than both the L1-integrator and Newmark’s method. Note that in the linear case investigated here, the integrals in the discrete momenta can be evaluated analytically, i.e. without numerical quadrature. For an example including Gaussian quadrature in time we refer to the nonlinear bar investigated in Section 6.2. In conclusion, for a certain required accuracy, our pp-scheme may be even faster than the Newmark algorithm.

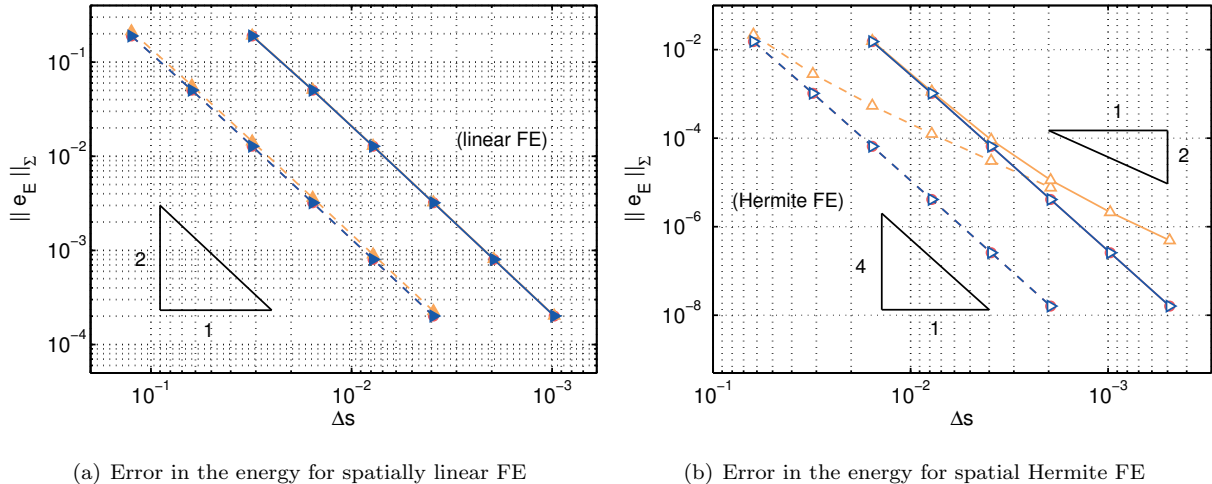


Figure 9: Linear elastic bar: Convergence behavior of the energy refining both the mesh and time step; the parameter Δs is given by $\Delta s = \Delta t/T_0^{\text{an}} = C_{\text{CFL}} \cdot \Delta L/(2L)$; shown are $C_{\text{CFL}} = 0.5$ (dashed line) $C_{\text{CFL}} = 0.125$ (solid line) for $T = 1T_0^{\text{an}}$.

	Newmark		L1-integrator		pp-scheme	
	Δs	T_{ct} [ms]	Δs	T_{ct} [ms]	Δs	T_{ct} [ms]
$\ e_u\ _{\Sigma} < 1\%$	1/32	79.6	1/32	105.0	1/16	44.9
$\ e_u\ _{\Sigma} < 0.1\%$	1/128	815.8	1/64	416.3	1/32	135.7
$\ e_u\ _{\Sigma} < 0.01\%$	1/256	2,919.4	1/256	5,381.3	1/64	574.3

Table 3: Linear elastic bar: Step size, Δs , and computation time, T_{ct} , of the test cases from Fig. 8(b) ($C_{\text{CFL}} = 0.5$), for which the error in the displacement is smaller than 1%, 0.1%, and 0.01%; T_{ct} denotes the computation time for one oscillation.

6.2. Deformation of a nonlinear bar

The numerical examples discussed in Section 5 and 6.1 cover both naturally discrete and (spatially discretized) continuum systems. So far, however, only linear problems (for which the internal forces depend on the displacement linearly) have been investigated. We therefore consider a nonlinear Neo-Hooke material behavior, which is described in Appendix D. The bar is initially deformed by prescribing the same displacement and velocity as in Section 6.1.1; see Eq. (62). Fig. 11 shows the deformation of the bar (a) at the very beginning and (b) after a long period of oscillations. Here, a Hermite finite element mesh with eight elements is chosen. For a better comparison with the results from the previous section, the time step is normalized by the period length of the first eigenmode, T_0^{an} . Since the mechanical response of the system differs from the linear case, however, the initially sinusoidal oscillations shown in Fig. 11(a) turn into a set of different interfering oscillations (Fig. 11(b)).

Fig. 12 shows the long-term behavior for a nonlinear bar, comparing the system's total energy for the

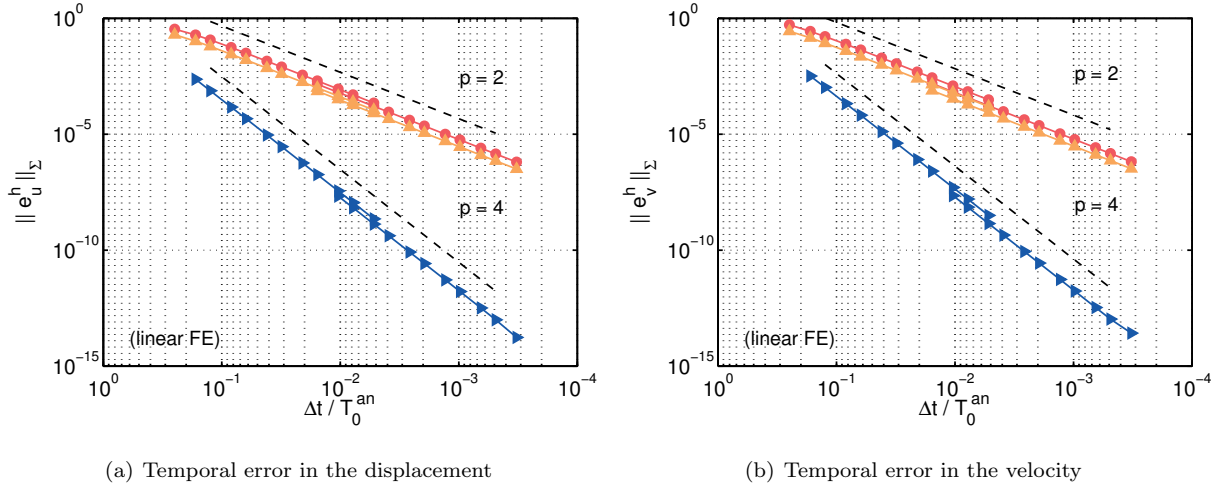


Figure 10: Linear elastic bar: Convergence of the temporal errors in the displacement and the velocity for linear Lagrange FE; $T = 1 T_0^{\text{an}}$, $\Delta t_0 = T_0^{\text{an}}/4$.

pp-scheme, the Newmark algorithm, and the L1-integrator. Like for the harmonic oscillator in Section 5.1, the energy oscillates while being qualitatively preserved. In comparison with the other methods the relative error of the pp-scheme is smaller by several orders of magnitude (Table 4).

Besides, we investigate the convergence behavior for a nonlinear bar, considering in space only Hermite finite elements. Since for this case the deformation cannot be computed analytically, we compare our results with a fine reference solution, using both a very fine FE mesh and a small time step. Like in the examples shown in the previous section, we simultaneously refine both discretizations. The results are shown in Fig. 13(a) – 13(c). The accuracy of our scheme becomes most apparent for the displacement and the total energy; for these quantities we observe a significantly higher convergence. Note that caused by the nonlinear material law, both the pp-scheme and the L1-integrator require numerical quadrature to evaluate the time integral over the internal forces; see also Appendix A.4. If we demand, however, a sufficient high accuracy w.r.t. the fine solution, the computational cost may still be lower for the pp-scheme than for the Newmark algorithm. An error in the displacement smaller than 10^{-5} (Fig. 13(a)), for instance, requires a step size of $\Delta s = 1/2048$ for Newmark’s method. In contrast, the pp-scheme achieves this accuracy already for $\Delta s = 1/512$. Therefore, the measured computation time is significantly lower: 48.7% of the time required for the Newmark algorithm.

We finally investigate for each refinement step how well the (spatially discrete) initial energy is preserved over time; see Fig. 13(d). The error plotted here thus arises only from the temporal discretization. A comparison with Fig. 6(c) shows that — for both the linear oscillator and the nonlinear bar — we achieve with the pp-scheme the same high order of convergence: $p = 4$.

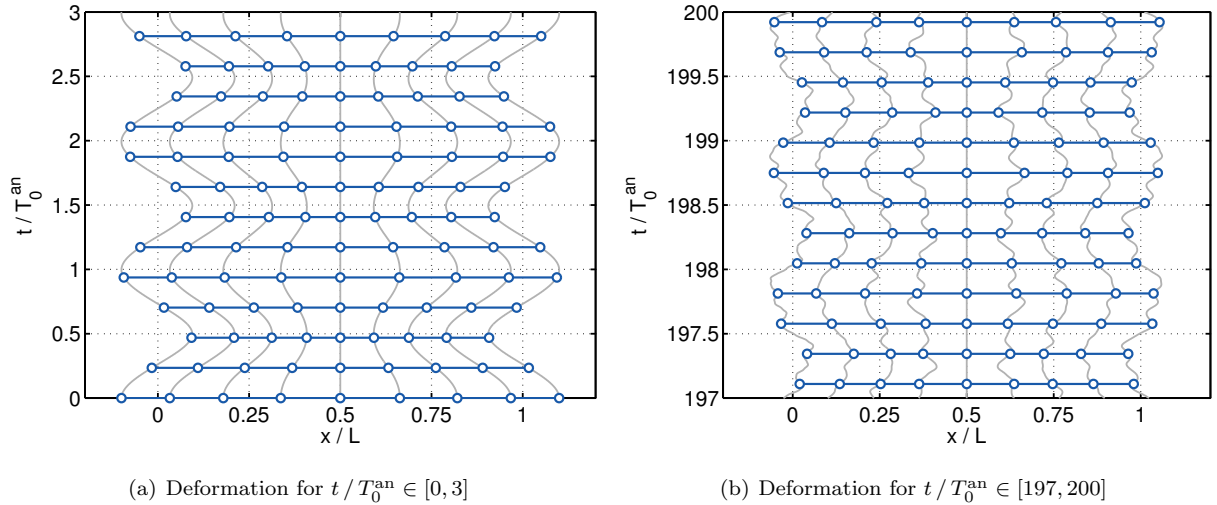


Figure 11: Nonlinear bar: Deformation of the bar (a) at the beginning of the oscillation, and (b) after a long time period, using the pp-scheme and Hermite FE; $T = 200 T_0^{\text{an}}$, $\Delta t = T_0^{\text{an}}/512$, $L_e = L/8$.

	NM	L1	pp
e_E^{max}	$1.09 \cdot 10^{-5}$	$4.93 \cdot 10^{-6}$	$3.72 \cdot 10^{-10}$

Table 4: Maximum values in the energy errors shown in Fig. 12; $e_E^{\text{max}} = \max |E(t_n) - E_0| / E_0$, $n = 0, \dots, N$.

7. Conclusion

In this work we derive a class of C^1 -continuous time integration methods for conservative elastodynamic problems. Using piecewise Hermite interpolation, we approximate the displacement of a deformable solid by C^1 -continuous functions in time. The velocity of the body is thus C^0 -continuous in the entire time domain. To explicitly account for any initial velocities in the system, we consider a generalization of Hamilton's principle, referred to as Hamilton's law of varying action. From the action integral of the continuous system we derive the spatially and temporally weak form of the equilibrium equation in elastodynamics. This expression is first discretized in space, using a standard (Galerkin) finite element method. Afterwards, the spatially discrete system is discretized in time by 1) subdividing the temporal domain into a set of smaller time intervals, and 2) approximating the displacement by cubic Hermite shape functions.

Generally, methods belonging to the class of variational integrators can be constructed by varying the action integral over the entire time domain. From this equation one can derive the discrete Euler-Lagrange equations in order to develop a subsequent time integration method. For cubic Hermite interpolation, however, the resulting variational integrator is unconditionally unstable. This issue has been discussed also by Riff and Baruch [61]. Therefore, we first vary the action of each time interval individually, and then derive different one-step methods to solve for the new (unknown) displacement and velocity. This yields

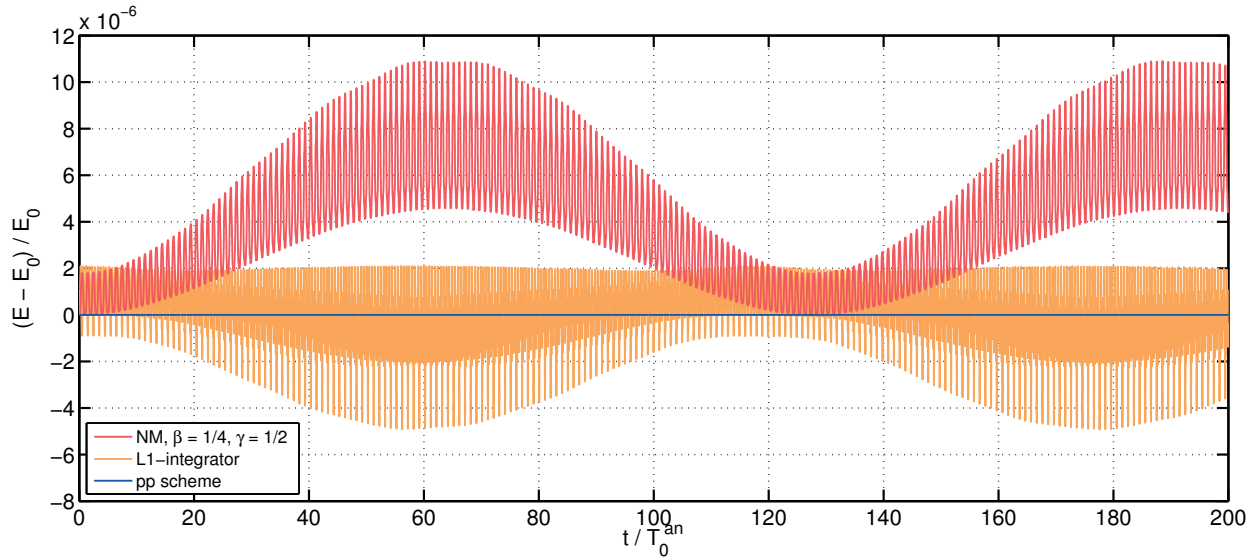


Figure 12: Nonlinear bar: Long-term energy behavior for approximately 200 periods of oscillation using Hermite FE; the maximum relative errors are listed in Tab. 4.; $\Delta t = T_0^{\text{an}}/256$, $L_e = L/4$.

six time integration schemes with different properties. Technically, these methods are not variational in the sense that they are not derived from the virtual action of the total domain. We show, however, that the most favorable of these methods — denoted as pp-scheme — offers the same advantageous properties like variational integrators: 1) Conservation of linear momentum, and 2) symplecticity for simple linear systems.

We first investigate the properties of our schemes by considering a harmonic oscillator. We then demonstrate numerically that the pp-scheme shows both conditional stability and convergence of order four. Afterwards, we examine both linear and nonlinear problems accounting either for inherently continuous or spatially discrete systems. Our results show that for an appropriate spatial discretization, the pp-scheme provides both reasonable computational effort and remarkably higher accuracy than variational integrators based on linear interpolation in time. This scheme also well-preserved the energy of the system for long-time integration. It remains to be seen whether our method is symplectic for arbitrary nonlinear systems. This should be considered in future investigations.

Since the scope of this work is both the construction and investigation of time integration methods, we here focus on one-dimensional elastodynamic problems. An elaborate study of elastodynamic problems in either two or three dimensions may be the scope of future work. In addition, since the numerical results obtained within this study for spatial Hermite finite elements look very promising, it would be interesting to apply our time integrator in combination with other spatially C^1 -continuous FE discretizations and — in particular — to isogeometric approaches [15, 33]. In contrast to higher-order Lagrangian finite elements, isogeometric elements can prevent high-frequency errors [16, 35] that require unnecessarily small time steps.

Acknowledgement

The authors are grateful to the German Research Foundation (DFG) supporting J. C. Mergel and R. A. Sauer through grants SA1822/5-1 and GSC111. They further thank Prof. Yuri B. Suris (Technical University of Berlin), Prof. Sachin S. Gautam (IIT Guwahati), and Marcus G. Schmidt (formerly RWTH Aachen University) for their helpful comments.

Appendix A. Implementation of our schemes

This section contains helpful details for the implementation of our time integration schemes.

Appendix A.1. Shape functions

In both the spatial and temporal discretizations, we consider either linear Lagrange or cubic Hermite shape functions. Usually, these functions are defined on master domains, denoted e.g. by $\tau \in [-1, 1]$ for the discretization in time. The mapping from the master to the temporal domain, $\tau \mapsto t$ ($t \in [t_n, t_{n+1}]$), is characterized by the Jacobian determinant $J_\tau := \partial t / \partial \tau$; this determinant is given by $J_\tau = (t_{n+1} - t_n) / 2$ for both the L1-integrator and our six schemes.

- Linear Lagrange shape functions (for the L1-integrator):

$$R_1(\tau) = \frac{1}{2}(1 - \tau), \quad R_2(\tau) = \frac{1}{2}(1 + \tau). \quad (\text{A.1})$$

- Cubic Hermite shape functions (for our schemes); see e.g. Ref. [71]:

$$\begin{aligned} R_1(\tau) &= \frac{1}{4}(2 + \tau)(1 - \tau)^2, & R_2(\tau) &= \frac{1}{4}(2 - \tau)(1 + \tau)^2, \\ H_1(\tau) &= \frac{J_\tau}{4}(\tau + 1)(1 - \tau)^2, & H_2(\tau) &= \frac{J_\tau}{4}(\tau - 1)(1 + \tau)^2. \end{aligned} \quad (\text{A.2})$$

Appendix A.2. Discrete Lagrangian and action integral

The discrete (pseudo-)momenta (30) and (31) are obtained by taking the derivatives of the spatially and temporally discrete action

$$\mathcal{S}^{ht} = \sum_{n=0}^{N-1} \mathcal{S}_{n+1}^{ht}, \quad \mathcal{S}_{n+1}^{ht} = \int_{t_n}^{t_{n+1}} L^{ht}(\mathbf{x}^t, \dot{\mathbf{x}}^t) dt. \quad (\text{A.3})$$

Here, the discrete Lagrangian, $L^{ht}(\mathbf{x}^t, \dot{\mathbf{x}}^t) = K^{ht}(\dot{\mathbf{x}}^t) - \Pi^{ht}(\mathbf{x}^t)$, can be determined from

$$K^{ht}(\dot{\mathbf{x}}^t) = \sum_{e=1}^{n_{e1}} \left[\frac{1}{2} (\dot{\mathbf{x}}_e^t)^\top \mathbf{m}_e \dot{\mathbf{x}}_e^t \right], \quad (\text{A.4})$$

$$\Pi^{ht}(\mathbf{x}^t) = \sum_{e=1}^{n_{e1}} \left[\int_{\Omega_0^e} W(\mathbf{x}_e^t) dV - (\mathbf{x}_e^t)^\top \mathbf{f}_{\text{ext}}^e(\mathbf{x}_e^t) \right]. \quad (\text{A.5})$$

In Eq. (32) – (35) we additionally use the relation $\mathbf{f}(\mathbf{x}^t) = \partial \Pi^{ht}(\mathbf{x}^t) / \partial \mathbf{x}^t$. If required, the discrete Hamiltonian of the system (i.e. the total energy) can be computed from

$$E^{ht}(\mathbf{x}^t, \dot{\mathbf{x}}^t) = K^{ht}(\dot{\mathbf{x}}^t) + \Pi^{ht}(\mathbf{x}^t). \quad (\text{A.6})$$

Appendix A.3. Derivatives of the discrete momenta

The derivatives of the discrete (pseudo-)momenta with respect to $\hat{\mathbf{x}}_{n+1}$ and $\hat{\mathbf{v}}_{n+1}$ are given by

$$\frac{\partial \hat{\mathbf{p}}_n^-}{\partial \hat{\mathbf{x}}_{n+1}} = -\mathbf{m} \int_{t_n}^{t_{n+1}} \dot{R}_1(t) \dot{R}_2(t) dt + \int_{t_n}^{t_{n+1}} R_1(t) R_2(t) \frac{\partial \mathbf{f}(\mathbf{x}^t)}{\partial \mathbf{x}^t} dt, \quad (\text{A.7})$$

$$\frac{\partial \hat{\mathbf{p}}_{n+1}^+}{\partial \hat{\mathbf{x}}_{n+1}} = \mathbf{m} \int_{t_n}^{t_{n+1}} \dot{R}_2^2(t) dt - \int_{t_n}^{t_{n+1}} R_2^2(t) \frac{\partial \mathbf{f}(\mathbf{x}^t)}{\partial \mathbf{x}^t} dt, \quad (\text{A.8})$$

$$\frac{\partial \hat{\mathbf{q}}_n^-}{\partial \hat{\mathbf{x}}_{n+1}} = -\mathbf{m} \int_{t_n}^{t_{n+1}} \dot{H}_1(t) \dot{R}_2(t) dt + \int_{t_n}^{t_{n+1}} H_1(t) R_2(t) \frac{\partial \mathbf{f}(\mathbf{x}^t)}{\partial \mathbf{x}^t} dt, \quad (\text{A.9})$$

$$\frac{\partial \hat{\mathbf{q}}_{n+1}^+}{\partial \hat{\mathbf{x}}_{n+1}} = \mathbf{m} \int_{t_n}^{t_{n+1}} \dot{H}_2(t) \dot{R}_2(t) dt - \int_{t_n}^{t_{n+1}} H_2(t) R_2(t) \frac{\partial \mathbf{f}(\mathbf{x}^t)}{\partial \mathbf{x}^t} dt \quad (\text{A.10})$$

and

$$\frac{\partial \hat{\mathbf{p}}_n^-}{\partial \hat{\mathbf{v}}_{n+1}} = -\mathbf{m} \int_{t_n}^{t_{n+1}} \dot{R}_1(t) \dot{H}_2(t) dt + \int_{t_n}^{t_{n+1}} R_1(t) H_2(t) \frac{\partial \mathbf{f}(\mathbf{x}^t)}{\partial \mathbf{x}^t} dt, \quad (\text{A.11})$$

$$\frac{\partial \hat{\mathbf{p}}_{n+1}^+}{\partial \hat{\mathbf{v}}_{n+1}} = \mathbf{m} \int_{t_n}^{t_{n+1}} \dot{R}_2(t) \dot{H}_2(t) dt - \int_{t_n}^{t_{n+1}} R_2(t) H_2(t) \frac{\partial \mathbf{f}(\mathbf{x}^t)}{\partial \mathbf{x}^t} dt, \quad (\text{A.12})$$

$$\frac{\partial \hat{\mathbf{q}}_n^-}{\partial \hat{\mathbf{v}}_{n+1}} = -\mathbf{m} \int_{t_n}^{t_{n+1}} \dot{H}_1(t) \dot{H}_2(t) dt + \int_{t_n}^{t_{n+1}} H_1(t) H_2(t) \frac{\partial \mathbf{f}(\mathbf{x}^t)}{\partial \mathbf{x}^t} dt, \quad (\text{A.13})$$

$$\frac{\partial \hat{\mathbf{q}}_{n+1}^+}{\partial \hat{\mathbf{v}}_{n+1}} = \mathbf{m} \int_{t_n}^{t_{n+1}} \dot{H}_2^2(t) dt - \int_{t_n}^{t_{n+1}} H_2^2(t) \frac{\partial \mathbf{f}(\mathbf{x}^t)}{\partial \mathbf{x}^t} dt. \quad (\text{A.14})$$

Appendix A.4. Analytical computation of the integrals

As pointed out in Section 4.3, some of the integrals in the discrete (pseudo-)momenta can be computed analytically. For this purpose, we split the internal force into a linear and into a nonlinear part,

$$\mathbf{f}_{\text{int}}(\mathbf{x}^t) = \mathbf{k} \mathbf{u}^t + \mathbf{f}_{\text{nl}}(\mathbf{x}^t), \quad (\text{A.15})$$

where $\mathbf{u}^t = \mathbf{x}^t - \mathbf{X}$, and where \mathbf{k} is a linear stiffness matrix. The case $\mathbf{f}_{\text{nl}} = \mathbf{0}$ corresponds to linear elasticity, while $\mathbf{k} = \mathbf{0}$ represents the fully nonlinear case. Further let

$$\tilde{\mathbf{f}}(\mathbf{x}^t) := \mathbf{f}_{\text{nl}}(\mathbf{x}^t) - \mathbf{f}_{\text{ext}}(\mathbf{x}^t). \quad (\text{A.16})$$

Inserting Eq. (24) and (25) into Eq. (40) – (43) yields with $\Delta t := t_{n+1} - t_n$

$$\begin{aligned} \hat{\mathbf{p}}_n^- &= \frac{1}{10 \Delta t} \mathbf{m} \left[12 \hat{\mathbf{u}}_{n+1} - 12 \hat{\mathbf{u}}_n - \Delta t \hat{\mathbf{v}}_{n+1} - \Delta t \hat{\mathbf{v}}_n \right] + \int_{t_n}^{t_{n+1}} R_1(t) \tilde{\mathbf{f}}(\mathbf{x}^t) dt \\ &\quad + \frac{\Delta t}{420} \mathbf{k} \left[54 \hat{\mathbf{u}}_{n+1} + 156 \hat{\mathbf{u}}_n - 13 \Delta t \hat{\mathbf{v}}_{n+1} + 22 \Delta t \hat{\mathbf{v}}_n \right], \end{aligned} \quad (\text{A.17})$$

$$\begin{aligned} \hat{\mathbf{p}}_{n+1}^+ &= \frac{1}{10 \Delta t} \mathbf{m} \left[12 \hat{\mathbf{u}}_{n+1} - 12 \hat{\mathbf{u}}_n - \Delta t \hat{\mathbf{v}}_{n+1} - \Delta t \hat{\mathbf{v}}_n \right] - \int_{t_n}^{t_{n+1}} R_2(t) \tilde{\mathbf{f}}(\mathbf{x}^t) dt \\ &\quad + \frac{\Delta t}{420} \mathbf{k} \left[-156 \hat{\mathbf{u}}_{n+1} - 54 \hat{\mathbf{u}}_n + 22 \Delta t \hat{\mathbf{v}}_{n+1} - 13 \Delta t \hat{\mathbf{v}}_n \right] \end{aligned} \quad (\text{A.18})$$

and

$$\begin{aligned} \hat{\mathbf{q}}_n^- &= \frac{1}{30} \mathbf{m} \left[3 \hat{\mathbf{u}}_{n+1} - 3 \hat{\mathbf{u}}_n + \Delta t \hat{\mathbf{v}}_{n+1} - 4 \Delta t \hat{\mathbf{v}}_n \right] + \int_{t_n}^{t_{n+1}} H_1(t) \tilde{\mathbf{f}}(\mathbf{x}^t) dt \\ &\quad + \frac{\Delta t^2}{420} \mathbf{k} \left[13 \hat{\mathbf{u}}_{n+1} + 22 \hat{\mathbf{u}}_n - 3 \Delta t \hat{\mathbf{v}}_{n+1} + 4 \Delta t \hat{\mathbf{v}}_n \right], \end{aligned} \quad (\text{A.19})$$

$$\begin{aligned} \hat{\mathbf{q}}_{n+1}^+ &= \frac{1}{30} \mathbf{m} \left[-3 \hat{\mathbf{u}}_{n+1} + 3 \hat{\mathbf{u}}_n + 4 \Delta t \hat{\mathbf{v}}_{n+1} - \Delta t \hat{\mathbf{v}}_n \right] - \int_{t_n}^{t_{n+1}} H_2(t) \tilde{\mathbf{f}}(\mathbf{x}^t) dt \\ &\quad + \frac{\Delta t^2}{420} \mathbf{k} \left[22 \hat{\mathbf{u}}_{n+1} + 13 \hat{\mathbf{u}}_n - 4 \Delta t \hat{\mathbf{v}}_{n+1} + 3 \Delta t \hat{\mathbf{v}}_n \right]. \end{aligned} \quad (\text{A.20})$$

The derivatives then simplify to

$$\frac{\partial \hat{\mathbf{p}}_n^-}{\partial \hat{\mathbf{x}}_{n+1}} = \frac{6}{5 \Delta t} \mathbf{m} + \frac{9 \Delta t}{70} \mathbf{k} + \int_{t_n}^{t_{n+1}} R_1(t) R_2(t) \frac{\partial \tilde{\mathbf{f}}(\mathbf{x}^t)}{\partial \mathbf{x}^t} dt, \quad (\text{A.21})$$

$$\frac{\partial \hat{\mathbf{p}}_{n+1}^+}{\partial \hat{\mathbf{x}}_{n+1}} = \frac{6}{5 \Delta t} \mathbf{m} - \frac{13 \Delta t}{35} \mathbf{k} - \int_{t_n}^{t_{n+1}} R_2^2(t) \frac{\partial \tilde{\mathbf{f}}(\mathbf{x}^t)}{\partial \mathbf{x}^t} dt, \quad (\text{A.22})$$

$$\frac{\partial \hat{\mathbf{q}}_n^-}{\partial \hat{\mathbf{x}}_{n+1}} = \frac{1}{10} \mathbf{m} + \frac{13 \Delta t^2}{420} \mathbf{k} + \int_{t_n}^{t_{n+1}} H_1(t) R_2(t) \frac{\partial \tilde{\mathbf{f}}(\mathbf{x}^t)}{\partial \mathbf{x}^t} dt, \quad (\text{A.23})$$

$$\frac{\partial \hat{\mathbf{q}}_{n+1}^+}{\partial \hat{\mathbf{x}}_{n+1}} = -\frac{1}{10} \mathbf{m} + \frac{11 \Delta t^2}{210} \mathbf{k} - \int_{t_n}^{t_{n+1}} H_2(t) R_2(t) \frac{\partial \tilde{\mathbf{f}}(\mathbf{x}^t)}{\partial \mathbf{x}^t} dt \quad (\text{A.24})$$

and

$$\frac{\partial \hat{\mathbf{p}}_n^-}{\partial \hat{\mathbf{v}}_{n+1}} = -\frac{1}{10} \mathbf{m} - \frac{13 \Delta t^2}{420} \mathbf{k} + \int_{t_n}^{t_{n+1}} R_1(t) H_2(t) \frac{\partial \tilde{\mathbf{f}}(\mathbf{x}^t)}{\partial \mathbf{x}^t} dt, \quad (\text{A.25})$$

$$\frac{\partial \hat{\mathbf{p}}_{n+1}^+}{\partial \hat{\mathbf{v}}_{n+1}} = -\frac{1}{10} \mathbf{m} + \frac{11 \Delta t^2}{210} \mathbf{k} - \int_{t_n}^{t_{n+1}} R_2(t) H_2(t) \frac{\partial \tilde{\mathbf{f}}(\mathbf{x}^t)}{\partial \mathbf{x}^t} dt, \quad (\text{A.26})$$

$$\frac{\partial \hat{\mathbf{q}}_n^-}{\partial \hat{\mathbf{v}}_{n+1}} = \frac{\Delta t}{30} \mathbf{m} - \frac{\Delta t^3}{140} \mathbf{k} + \int_{t_n}^{t_{n+1}} H_1(t) H_2(t) \frac{\partial \tilde{\mathbf{f}}(\mathbf{x}^t)}{\partial \mathbf{x}^t} dt, \quad (\text{A.27})$$

$$\frac{\partial \hat{\mathbf{q}}_{n+1}^+}{\partial \hat{\mathbf{v}}_{n+1}} = \frac{2 \Delta t}{15} \mathbf{m} - \frac{\Delta t^3}{105} \mathbf{k} - \int_{t_n}^{t_{n+1}} H_2^2(t) \frac{\partial \tilde{\mathbf{f}}(\mathbf{x}^t)}{\partial \mathbf{x}^t} dt. \quad (\text{A.28})$$

Appendix B. Linear variational integrator (L1)

This section outlines the linear variational integrator (L1) that we use for comparison in Section 5 and 6. Here, the deformation is approximated by $\mathbf{x}(t) \approx \mathbf{x}^t(t)$,

$$\mathbf{x}^t(t) = R_1(t) \hat{\mathbf{x}}_n + R_2(t) \hat{\mathbf{x}}_{n+1}, \quad t \in [t_n, t_{n+1}], \quad (\text{B.1})$$

where R_1 and R_2 are defined by Eq. (A.1). In analogy, we introduce

$$\delta \mathbf{x}^t(t) = R_1(t) \delta \hat{\mathbf{x}}_n + R_2(t) \delta \hat{\mathbf{x}}_{n+1}, \quad (\text{B.2})$$

$$\dot{\mathbf{x}}^t(t) = \dot{R}_1(t) \hat{\mathbf{x}}_n + \dot{R}_2(t) \hat{\mathbf{x}}_{n+1}, \quad (\text{B.3})$$

$$\delta \dot{\mathbf{x}}^t(t) = \dot{R}_1(t) \delta \hat{\mathbf{x}}_n + \dot{R}_2(t) \delta \hat{\mathbf{x}}_{n+1}. \quad (\text{B.4})$$

With this interpolation the discretized action becomes $\mathcal{S}^h \approx \mathcal{S}^{ht}$,

$$\mathcal{S}^{ht} = \sum_{n=0}^{N-1} \mathcal{S}_{n+1}^{ht}(\hat{\mathbf{x}}_n, \hat{\mathbf{x}}_{n+1}). \quad (\text{B.5})$$

From the discretization of the virtual action then follows that

$$\sum_{n=0}^{N-1} \left[\frac{\partial \mathcal{S}_{n+1}^{ht}}{\partial \hat{\mathbf{x}}_n} \delta \hat{\mathbf{x}}_n + \frac{\partial \mathcal{S}_{n+1}^{ht}}{\partial \hat{\mathbf{x}}_{n+1}} \delta \hat{\mathbf{x}}_{n+1} \right] = \delta \mathbf{x}_N \cdot \mathbf{m} \dot{\mathbf{x}}^t(T) - \delta \mathbf{x}_0 \cdot \mathbf{m} \dot{\mathbf{x}}^t(0). \quad (\text{B.6})$$

Since the n^{th} time step belongs to two time intervals, $\mathcal{T}^n = [t_{n-1}, t_n]$ and $\mathcal{T}^{n+1} = [t_n, t_{n+1}]$, we obtain

$$\mathbf{m} \dot{\mathbf{x}}^t(0) + \frac{\partial \mathcal{S}_1^{ht}(\hat{\mathbf{x}}_0, \hat{\mathbf{x}}_1)}{\partial \hat{\mathbf{x}}_0} = \mathbf{0}, \quad (\text{B.7})$$

$$\frac{\partial \mathcal{S}_n^{ht}(\hat{\mathbf{x}}_{n-1}, \hat{\mathbf{x}}_n)}{\partial \hat{\mathbf{x}}_n} + \frac{\partial \mathcal{S}_{n+1}^{ht}(\hat{\mathbf{x}}_n, \hat{\mathbf{x}}_{n+1})}{\partial \hat{\mathbf{x}}_n} = \mathbf{0}, \quad n = 1, \dots, N-1. \quad (\text{B.8})$$

The integrals within the partial derivatives of \mathcal{S}_{n+1}^{ht} are also evaluated by Gaussian quadrature.

Appendix C. Amplification matrices for the simple harmonic oscillator

The amplification matrices of our six schemes (44) – (49) (required for Eq. (52)) are given by

$$\begin{aligned} \mathbf{A}_{\text{pp}} &= \frac{1}{8\gamma^4 + 132\gamma^2 + 2016} \begin{bmatrix} (26\gamma^4 - 876\gamma^2 + 2016) & (204\gamma^3 - 2016\gamma) \\ (3\gamma^5 - 204\gamma^3 + 2016\gamma) & (26\gamma^4 - 876\gamma^2 + 2016) \end{bmatrix}, \\ \mathbf{A}_{\text{qq}} &= \frac{1}{2\gamma^4 + 18\gamma^2 + 420} \begin{bmatrix} (7\gamma^4 - 192\gamma^2 + 420) & (45\gamma^3 - 420\gamma) \\ (\gamma^5 - 52\gamma^3 + 420\gamma) & (7\gamma^4 - 192\gamma^2 + 420) \end{bmatrix}, \\ \mathbf{A}_{\text{p}^+\text{q}^-} &= \frac{1}{26\gamma^4 + 198\gamma^2 + 3780} \begin{bmatrix} (65\gamma^4 - 1692\gamma^2 + 3780) & (390\gamma^3 - 3780\gamma) \\ (7\gamma^5 - 432\gamma^3 + 3780\gamma) & (46\gamma^4 - 1692\gamma^2 + 3780) \end{bmatrix}, \\ \mathbf{A}_{\text{p}^+\text{q}^+} &= \frac{1}{10\gamma^4 + 24\gamma^2 + 630} \begin{bmatrix} (13\gamma^4 - 291\gamma^2 + 630) & (60\gamma^3 - 630\gamma) \\ (\gamma^5 - 81\gamma^3 + 630\gamma) & (5\gamma^4 - 291\gamma^2 + 630) \end{bmatrix}, \\ \mathbf{A}_{\text{p}^-\text{q}^-} &= \frac{1}{\gamma^4 + 48\gamma^2 + 1260} \begin{bmatrix} (10\gamma^4 - 582\gamma^2 + 1260) & (120\gamma^3 - 1260\gamma) \\ (2\gamma^5 - 162\gamma^3 + 1260\gamma) & (26\gamma^4 - 582\gamma^2 + 1260) \end{bmatrix}, \\ \mathbf{A}_{\text{p}^-\text{q}^+} &= \frac{1}{10\gamma^4 + 198\gamma^2 + 3780} \begin{bmatrix} (46\gamma^4 - 1692\gamma^2 + 3780) & (390\gamma^3 - 3780\gamma) \\ (7\gamma^5 - 432\gamma^3 + 3780\gamma) & (65\gamma^4 - 1692\gamma^2 + 3780) \end{bmatrix}. \end{aligned}$$

Appendix D. Equations for the 1D bar

In Section 6 we investigate the axial deformation of a thin bar that is characterized by its length, L , density, ρ_0 , cross section area, A , and Young's modulus, E . We study both linear and nonlinear problems by considering different material behavior for the bar. For these examples the external forces, and thus the variation $\delta\Pi_{\text{ext}}$, are both zero. Let X , x , and v denote the 1D equivalents of the terms written in bold font. For the 1D case the virtual kinetic energy, given by Eq. (8), reduces to

$$\delta K(v) = \rho_0 A \int_0^L \delta v \cdot v \, dX. \quad (\text{D.1})$$

For a linear elastic bar (discussed in Section 6.1), the virtual internal work (9) is given by

$$\delta\Pi_{\text{int}}(x) = A \int_0^L \delta\varepsilon \cdot E \varepsilon \, dX, \quad \varepsilon := \lambda - 1, \quad (\text{D.2})$$

where $\lambda := \partial x / \partial X$. In Section 6.2 we consider a Neo-Hooke material with Poisson's ratio $\nu = 0$; see e.g. Ref. [73]:

$$\delta\Pi_{\text{int}}(x) = A \int_0^L \delta\lambda \cdot P \, dX, \quad P := \frac{E}{2} (\lambda - \lambda^{-1}). \quad (\text{D.3})$$

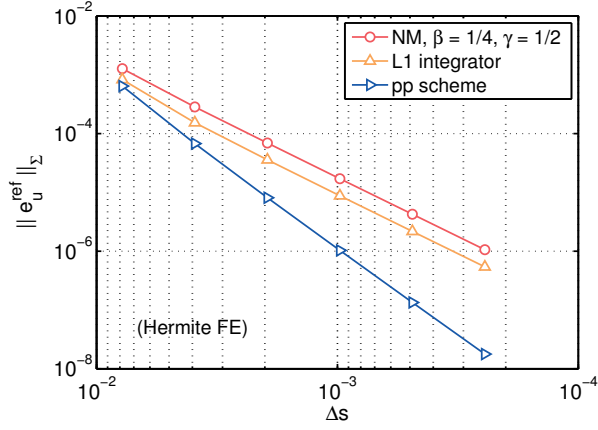
For the spatial discretization of Eq. (D.1) – (D.3) by means of 1D finite elements, we refer e.g. to Ref. [71].

References

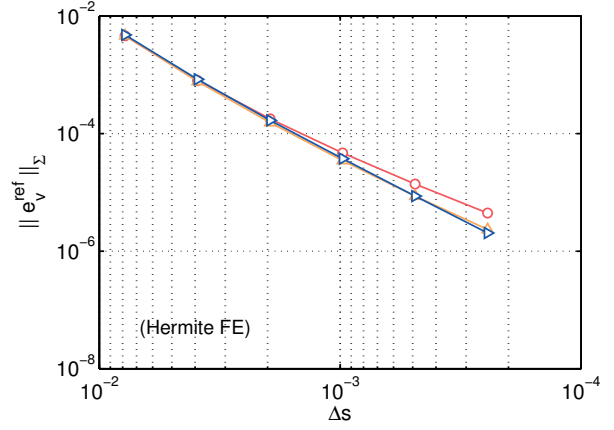
- [1] J. H. Argyris, D. W. Scharpf, Finite elements in time and space, *Nucl. Eng. Des.* **10** (1969) 456–464.
- [2] C. D. Bailey, Application of Hamilton’s law of varying action, *AIAA Journal* **13** (9) (1975) 1154–1157.
- [3] C. D. Bailey, A new look at Hamilton’s principle, *Found. Phys.* **5** (3) (1975) 433–451.
- [4] C. D. Bailey, Hamilton, Ritz, and elastodynamics, *J. Appl. Mech.* **43** (4) (1976) 684–688.
- [5] C. D. Bailey, The method of Ritz applied to the equation of Hamilton, *Comput. Meth. Appl. Mech. Engrg.* **7** (1976) 235–247.
- [6] M. Baruch, R. Riff, Hamilton’s principle, Hamilton’s law – 6th correct formulations, *AIAA Journal* **20** (5) (1982) 687–692.
- [7] O. A. Bauchau, T. Joo, Computational schemes for non-linear elasto-dynamics, *Int. J. Numer. Meth. Engrg.* **45** (1999) 693–719.
- [8] T. Belytschko, W. K. Liu, B. Moran, *Nonlinear Finite Elements for Continua and Structures*, Wiley, 2000.
- [9] P. Betsch, P. Steinmann, Conserving properties of a time FE method – part II: Time-stepping schemes for non-linear elastodynamics, *Int. J. Numer. Meth. Engrg.* **50** (2001) 1931–1955.
- [10] M. Borri, G. L. Ghiringhelli, M. Lanz, P. Mantegazza, T. Merlini, Dynamic response of mechanical systems by a weak Hamiltonian formulation, *Comput. Struct.* **20** (1-3) (1985) 495–508.
- [11] N. Bou-Rabee, H. Owhadi, Stochastic variational integrators, *IMA J. Numer. Anal.* **29** (2008) 421–443.
- [12] P. Chadwick, *Continuum Mechanics: Concise Theory and Problems*, Dover Publications, 1999.
- [13] J. Chung, G. M. Hulbert, A time integration algorithm for structural dynamics with improved numerical dissipation: The generalized- α method, *J. Appl. Mech.* **60** (1993) 371–375.
- [14] J. Cortés, S. Martínez, Non-holonomic integrators, *Nonlinearity* **14** (5) (2001) 1365–1392.
- [15] J. A. Cottrell, T. J. R. Hughes, Y. Bazilevs, *Isogeometric Analysis*, Wiley, 2009.
- [16] J. A. Cottrell, A. Reali, Y. Bazilevs, T. J. R. Hughes, Isogeometric analysis of structural vibrations, *Comput. Meth. Appl. Mech. Engrg.* **195** (2006) 5257–5296.
- [17] F. Demoures, F. Gay-Balmaz, S. Leyendecker, S. Ober-Blöbaum, T. S. Ratiu, Y. Weinand, Discrete variational Lie group formulation of geometrically exact beam dynamics, *Numer. Math.* **130** (1) (2014) 73–123.
- [18] R. C. Fetecau, J. E. Marsden, M. Ortiz, M. West, Nonsmooth Lagrangian mechanics and variational collision integrators, *SIAM J. Appl. Dyn. Syst.* **2** (3) (2003) 381–416.
- [19] I. Fried, Finite-element analysis of time-dependent phenomena, *AIAA Journal* **7** (6) (1969) 1170–1173.
- [20] T. C. Fung, Unconditionally stable higher-order accurate Hermitian time finite elements, *Int. J. Numer. Meth. Engrg.* **39** (1996) 3475–3495.
- [21] S. S. Gautam, R. A. Sauer, An energy-momentum-conserving temporal discretization scheme for adhesive contact problems, *Int. J. Numer. Meth. Engrg.* **93** (10) (2013) 1057–1081.
- [22] M. Géradin, On the variational method in the direct integration of the transient structural response, *J. Sound Vib.* **34** (4) (1974) 479–487.
- [23] O. Gonzalez, Exact energy and momentum conserving algorithms for general models in nonlinear elasticity, *Comput. Meth. Appl. Mech. Engrg.* **190** (2000) 1763–1783.
- [24] M. Groß, P. Betsch, P. Steinmann, Conservation properties of a time FE method – part IV: Higher order energy and momentum conserving schemes, *Int. J. Numer. Meth. Engrg.* (2005) 1849–1897.
- [25] E. Hairer, C. Lubich, G. Wanner, *Geometric Numerical Integration*, 2nd ed., Springer, Berlin Heidelberg, 2006.
- [26] W. R. Hamilton, On a general method in dynamics; by which the study of the motions of all free systems of attracting or repelling points is reduced to the search and differentiation of one central relation, or characteristic function, *Phil. Trans. R. Soc. Lond.* **124** (1834) 247–308.
- [27] W. R. Hamilton, Second essay on a general method in dynamics, *Phil. Trans. R. Soc. Lond.* **125** (1835) 95–144.

- [28] C. Hesch, P. Betsch, A mortar method for energy-momentum conserving schemes in frictionless dynamic contact problems, *Int. J. Numer. Meth. Engrg.* **77** (2009) 1468–1500.
- [29] C. Hesch, P. Betsch, Transient three-dimensional domain decomposition problems: Frame-indifferent mortar constraints and conserving integration, *Int. J. Numer. Meth. Engrg.* **82** (2010) 329–358.
- [30] H. M. Hilber, T. J. R. Hughes, R. L. Taylor, Improved numerical dissipation for time integration algorithms in structural dynamics, *Earthq. Eng. Struct. Dyn* **5** (1977) 283–292.
- [31] G. A. Holzapfel, *Nonlinear Solid Mechanics: A Continuum Approach for Engineering*, Wiley, 2000.
- [32] T. J. R. Hughes, Stability, convergence and growth and decay of energy of the average acceleration method in nonlinear structural dynamics, *Comput. Struct.* **6** (1976) 313–324.
- [33] T. J. R. Hughes, J. A. Cottrell, Y. Bazilevs, Isogeometric analysis: CAD, finite elements, NURBS, exact geometry and mesh refinement, *Comp. Meth. Appl. Mech. Engrg.* **194** (2005) 4135–4195.
- [34] T. J. R. Hughes, G. M. Hulbert, Space-time finite element methods for elastodynamics: Formulations and error estimates, *Comput. Meth. Appl. Mech. Engrg.* **66** (1988) 339–363.
- [35] T. J. R. Hughes, A. Reali, G. Sangalli, Duality and unified analysis of discrete approximations in structural dynamics and wave propagation: Comparison of p -method finite elements with k -method NURBS, *Comput. Meth. Appl. Mech. Engrg.* **197** (2008) 4104–4124.
- [36] G. M. Hulbert, Time finite element methods for structural dynamics, *Int. J. Numer. Meth. Engrg.* **33** (1992) 307–331.
- [37] G. M. Hulbert, T. J. R. Hughes, Space-time finite element methods for second-order hyperbolic equations, *Comput. Meth. Appl. Mech. Engrg.* **84** (3) (1990) 327–348.
- [38] G. Johnson, S. Leyendecker, M. Ortiz, Discontinuous variational time integrators for complex multibody collisions, *Int. J. Numer. Meth. Engrg.* **100** (2014) 871–913.
- [39] C. Kane, J. E. Marsden, M. Ortiz, M. West, Variational integrators and the Newmark algorithm for conservative and dissipative mechanical systems, *Int. J. Numer. Meth. Engrg.* **49** (2000) 1295–1325.
- [40] M. Kobilarov, J. E. Marsden, G. S. Sukhatme, Geometric discretization of nonholonomic systems with symmetries, *Discrete Contin. Dyn. Syst. Ser. S* **1** (1) (2010) 61–84.
- [41] S. Krenk, Energy conservation in Newmark based time integration algorithms, *Comput. Meth. Appl. Mech. Engrg.* **195** (2006) 6110–6124.
- [42] S. Krenk, Global format for energy-momentum based time integration in nonlinear dynamics, *Int. J. Numer. Meth. Engrg.* **100** (2014) 458–476.
- [43] C. Lanczos, *The Variational Principles of Mechanics*, 4th ed., Dover Publications, New York, 1970.
- [44] B. Leimkuhler, S. Reich, *Simulating Hamiltonian dynamics*, Cambridge University Press, 2004.
- [45] M. Leok, T. Shingel, Prolongation-collocation variational integrators, *IMA J. Numer. Anal.* **32** (3) (2012) 1194–1216.
- [46] A. Lew, J. E. Marsden, M. Ortiz, M. West, Asynchronous variational integrators, *Arch. Rational Mech. Anal.* **167** (2) (2003) 85–146.
- [47] A. Lew, J. E. Marsden, M. Ortiz, M. West, An overview of variational integrators, in: L. P. Franca, T. E. Tezduyar, A. Masud (eds.), *Finite Element Methods: 1970’s and Beyond*, CIMNE, Barcelona, 2004, pp. 98–115.
- [48] A. Lew, J. E. Marsden, M. Ortiz, M. West, Variational time integrators, *Int. J. Numer. Meth. Engrg.* **60** (1) (2004) 153–212.
- [49] S. Leyendecker, J. E. Marsden, M. Ortiz, Variational integrators for constrained dynamical systems, *J. Appl. Math. Mech.* **88** (9) (2008) 677–708.
- [50] S. Leyendecker, S. Ober-Blöbaum, A variational approach to multirate integration for constrained systems, in: J.-C. Samin, P. Fiset (eds.), *Multibody Dynamics*, vol. 28 of *Computational Methods in Applied Sciences*, Springer Netherlands, 2013, pp. 97–121.

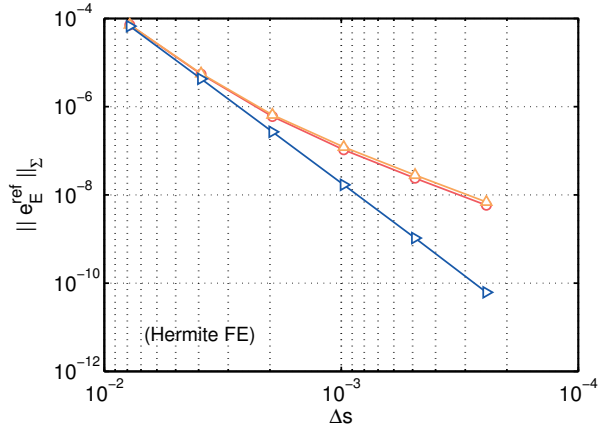
- [51] S. Leyendecker, S. Ober-Blöbaum, J. E. Marsden, M. Ortiz, Discrete mechanics and optimal control for constrained systems, *Optimal Control, Applications and Methods* **31** (6) (2010) 505–528.
- [52] J. E. Marsden, G. W. Patrick, S. Shkoller, Multisymplectic geometry, variational integrators, and nonlinear PDEs, *Commun. Math. Phys.* **199** (2) (1998) 351–395.
- [53] J. E. Marsden, M. West, Discrete mechanics and variational integrators, *Acta Numer.* **10** (2001) 357–514.
- [54] S. Modak, E. D. Sotelino, The generalized method for structural dynamics applications, *Adv. Eng. Softw.* **33** (2002) 565–575.
- [55] N. M. Newmark, A method of computation for structural dynamics, *ASCE J. Eng. Mech. Div.* **85** (EM3) (1959) 67–94.
- [56] S. Ober-Blöbaum, O. Junge, J. E. Marsden, Discrete mechanics and optimal control: an analysis, *Control Optim. Calc. Var.* **17** (2) (2011) 322–352.
- [57] S. Ober-Blöbaum, N. Saake, Construction and analysis of higher order Galerkin variational integrators, *Advances in Computational Mathematics* (2014) DOI: 10.1007/s10444-014-9394-8.
- [58] S. Ober-Blöbaum, M. Tao, M. Cheng, H. Owhadi, J. E. Marsden, Variational integrators for electric circuits, *J. Comput. Phys.* **242** (C) (2013) 498–530.
- [59] J. T. Oden, A general theory of finite elements II. Applications, *Int. J. Numer. Meth. Engrg.* **1** (1969) 247–259.
- [60] S. Reich, Momentum conserving symplectic integrations, *Physica D* **76** (4) (1994) 375–383.
- [61] R. Riff, M. Baruch, Stability of time finite elements, *AIAA Journal* **22** (8) (1984) 1171–1173.
- [62] R. Riff, M. Baruch, Time finite element discretization of Hamilton’s law of varying action, *AIAA Journal* **22** (9) (1984) 1310–1318.
- [63] T. E. Simkins, Unconstrained variational statements for initial and boundary-value problems, *AIAA Journal* **16** (6) (1978) 559–563.
- [64] T. E. Simkins, Finite elements for initial value problems in dynamics, *AIAA Journal* **19** (10) (1981) 1357–1362.
- [65] J. C. Simo, N. Tarnow, The discrete energy-momentum method. Conserving algorithms for nonlinear elastodynamics, *Z. Angew. Math. Phys.* **43** (1992) 757–792.
- [66] J. C. Simo, N. Tarnow, K. K. Wong, Exact energy-momentum conserving algorithms and symplectic schemes for nonlinear dynamics, *Comput. Meth. Appl. Mech. Engrg.* **100** (1) (1992) 63–116.
- [67] Y. B. Suris, Hamiltonian methods of Runge-Kutta type and their variational interpretation, *Math. Model.* **2** (1990) 78–87.
- [68] M. Tao, H. Owhadi, J. E. Marsden, Nonintrusive and structure preserving multiscale integration of stiff ODEs, SDEs, and Hamiltonian systems with hidden slow dynamics via flow averaging, *Multiscale Model. Simul.* **8** (4) (2010) 1269–1324.
- [69] S. Wolff, C. Buchner, Asynchronous variational integration using continuous assumed gradient elements, *Comput. Meth. Appl. Mech. Engrg.* **255** (2013) 158–166.
- [70] W. L. Wood, M. Bossak, O. C. Zienkiewicz, An alpha modification of Newmark’s method, *Int. J. Numer. Meth. Engrg.* **15** (1980) 1562–1566.
- [71] P. Wriggers, *Nonlinear Finite Element Methods*, Springer, Berlin Heidelberg, 2008.
- [72] O. C. Zienkiewicz, A new look at the Newmark, Houbolt and other time stepping formulas. A weighted residual approach, *Earthq. Eng. Struct. Dyn.* **5** (4) (1977) 413–418.
- [73] O. C. Zienkiewicz, R. L. Taylor, *The Finite Element Method for Solid and Structural Mechanics*, 6th ed., Butterworth-Heinemann, 2005.



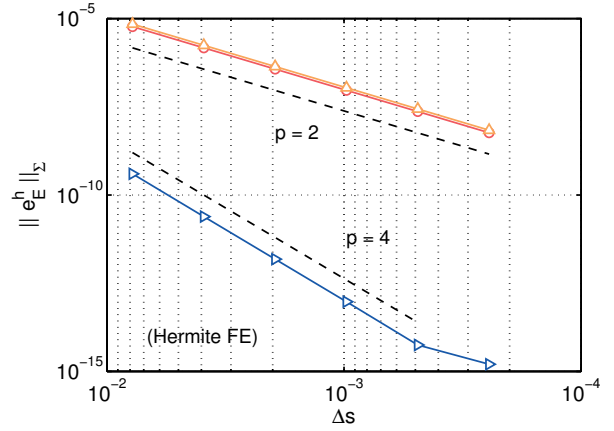
(a) Error in the displacement (w.r.t. reference solution)



(b) Error in the velocity (w.r.t. reference solution)



(c) Error in the total energy (w.r.t. reference solution)



(d) Error in the total energy (w.r.t. E_0)

Figure 13: Nonlinear bar: Relative errors with respect to (a) – (c) a very fine reference solution and (d) to the initial energy of the spatially discrete system, refining both the mesh and time step; $\Delta s = \Delta t/T_0^{\text{an}} = \Delta L/(16L)$; shown is $C_{\text{ CFL}} = 0.125$ for Hermite FE and $T = 2T_0^{\text{an}}$; the reference solution is computed with the pp-scheme using $L_e^{\text{ref}} = L/256$ and $\Delta t^{\text{ref}} = T_0^{\text{an}}/8192$.